

1 **Holocene sea-level database from the Atlantic coast of Europe**

2 Ane García-Artola^{1,2*}, Pierre Stéphan³, Alejandro Cearreta^{2,4}, Robert E. Kopp⁵, Nicole S. Khan¹,
3 and Benjamin P. Horton^{1,6}

4 ¹Asian School of the Environment, Nanyang Technological University, Singapore

5 ²Departamento de Estratigrafía y Paleontología, Universidad del País Vasco UPV/EHU, Bilbao,
6 Spain

7 ³CNRS, laboratoire LETG, Institut Universitaire Européen de la Mer, Université de Bretagne
8 Occidentale, Plouzané, France

9 ⁴Basque Centre for Climate Change-BC3, Leioa, Spain

10 ⁵Department of Earth and Planetary Sciences and Institute of Earth, Ocean and Atmospheric
11 Sciences, Rutgers University, New Brunswick, NJ, USA

12 ⁶Earth Observatory of Singapore, Nanyang Technological University, Singapore

13 *ane.garcia@ehu.eus

14 **Abstract**

15 We present a Holocene relative sea-level (RSL) database for the Atlantic coast of Europe (ACE)
16 and estimate rates of RSL change from the ACE database using a spatio-temporal empirical
17 hierarchical model. The database contains 214 index points, which locate the RSL position in space
18 and time, and 126 limiting dates, which constrain RSL to above or below a certain elevation at a
19 specific point in time. The temporal distribution extends from present to ~11.5 ka, with only 42

20 index points older than 7 ka. The spatial distribution spans 1700 km from French Flanders (France)
21 to Algarve (Portugal), with more than half of the index points concentrated along the French coast.
22 The ACE database shows RSL was below present during the Holocene. Rates of RSL change were
23 highest during the early Holocene, ranging between $6.8 \pm 0.5 \text{ mm yr}^{-1}$ in middle Portugal and 6.3
24 $\pm 0.8 \text{ mm yr}^{-1}$ in southern France from 10 to 7 ka. Mid- to late-Holocene rates decreased over time
25 up to $0.1 \pm 0.5 \text{ mm yr}^{-1}$ in middle Portugal since 4 ka, due primarily to reduced input of meltwater.
26 Comparison of the data to output from a glacial-isostatic adjustment model indicates that
27 deglaciation of the British-Irish and Fennoscandian Ice Sheets dominate the large-scale variability
28 captured by the ACE database, which reflects a decreasing influence of the collapsing British-Irish
29 and Fennoscandian peripheral forebulge that migrated from the northeast to the northwest after ~ 4
30 ka.

31

32 **Keywords:** Relative sea level, Holocene, hierarchical statistical modeling, glacial-isostatic
33 adjustment, Atlantic Coast of Europe

34 **1. Introduction**

35 Modern sea-level rise associated with contemporary climate warming represents one of the most
36 important challenges facing coastal communities (Church et al., 2013; Hinkel et al., 2015; Mengel
37 et al., 2016; Chen et al., 2017). The sea-level rise hazard is not uniform, but instead reflects spatial
38 variability in the rate of relative sea-level rise (Nicholls et al., 2014; Love et al., 2016). Local
39 relative sea level (RSL: height of the sea surface with respect to the surface of the solid Earth) can

40 differ considerably from the global mean value because of vertical land motion and geoid change
41 caused by a variety of processes, including the surface loading response to past glacial-isostatic
42 adjustment (GIA) and contemporary land ice mass changes, tectonics, atmosphere-ocean dynamics
43 that affect the height of the sea surface relative to the geoid, and local processes such as sediment
44 compaction and tidal-range change (Milne et al., 2009; Kopp et al., 2015).

45 During the Last Glacial Maximum, large ice sheets covered high-latitude regions bordering the
46 North Atlantic (Laurentide, Fennoscandian and British-Irish Ice Sheets), causing land subsidence
47 beneath the ice sheet and uplift of the land surface/ocean floor in peripheral regions, the so-called
48 “proglacial forebulge” (Peltier, 1996; Lambeck et al., 2014). During deglaciation, the viscoelastic
49 response of the Earth reversed and regions beneath the ice sheets underwent isostatic uplift, while
50 the forebulge collapsed, causing subsidence (Peltier, 1996, 2004; Mitrovica and Milne, 2002). RSL
51 records have been subdivided into near- (beneath ice sheets), intermediate- (peripheral to ice
52 sheets), and far-field (distal to ice sheets) regions in response to the differing GIA signals (Khan
53 et al., 2015).

54 Holocene RSL databases have been constructed from near-, intermediate- and far-field regions in
55 North America (Engelhart and Horton, 2012; Engelhart et al., 2015), the Caribbean (Milne and
56 Peros, 2013; Khan et al., 2017), Europe (Lambeck et al., 1998; Brooks and Edwards, 2006; Vacchi
57 et al., 2016) and elsewhere (Horton et al., 2005). These databases provide crucial constraints for
58 parameters of Earth and ice components of GIA models, which cannot be estimated from direct
59 measurements (Milne and Peros, 2013; Roy and Peltier, 2015; Bradley et al., 2016). These
60 databases have been constructed following the standardized methodology developed by the

61 International Geological Correlation Projects (IGCP) 61, 200, 495, and 588 (e.g., Preuss, 1979;
62 Tooley, 1982; Shennan and Horton, 2002; Hijma et al., 2015).

63 In Europe, the RSL database from Great Britain and Ireland represents near- and intermediate-
64 field locations mainly associated with the GIA response to the British-Irish Ice Sheet (Shennan
65 and Horton, 2002; Brooks and Edwards, 2006; Bradley et al., 2011). Leorri et al. (2012a,b)
66 compared RSL histories in a few locations (i.e., Brittany, France; Basque Country, Spain; Minho,
67 Tagus Valley, and Algarve, Portugal) from the Atlantic coast of Europe (ACE) to the GIA model
68 developed by Bradley et al. (2011). They identified a north-south GIA gradient that extends from
69 northern France to the south of Portugal. However, Goslin et al. (2013, 2015) highlighted the
70 unreliability of some of the data from the Brittany region used by Leorri et al. (2012a) to validate
71 the GIA model predictions. Stéphan and Goslin (2014) reinterpreted the results from Leorri et al.
72 (2012a) to develop a Holocene RSL database for the Atlantic coast of France, but they did not
73 compare their data with output from a GIA model. Similar to the limitations of the French data
74 used by Leorri et al. (2012a), there exist some incorrectly located samples within their Spanish
75 dataset. Moreover, Leorri et al. (2012a) seem to have interpreted sample depths as RSL positions
76 in their reconstructions from the southern Portugal data by Teixeira et al. (2005). Therefore, new
77 studies are needed to better constrain RSL changes along the ACE and the influence of GIA.

78 Here, we reinterpret/validate previous compilations (Leorri et al., 2012a; Stéphan and Goslin,
79 2014) and incorporate new reconstructions to produce the first standardized Holocene RSL
80 database for the ACE. The goal of constructing the present database is to better understand the
81 spatially-variable RSL history and influence of GIA along the ACE. Our database consists of 214
82 sea-level index points and 126 limiting data from northern France (51.1°N and 2.5°E) to southern

83 Portugal (37°N and 8°W) (Fig. 1). We subdivide the database into 13 regions based on distance
84 from the British-Irish and Fennoscandian Ice Sheets. We account for the influence of sediment
85 compaction and explain sources of vertical and temporal uncertainty. We apply a spatio-temporal
86 empirical hierarchical model (Kopp et al., 2016) to analyze the spatial variability and the rates of
87 RSL change and compare the observations with predictions from the Bradley et al. (2016) GIA
88 model.

89 **2. Study area**

90 The ACE database covers most of the French, northern Spain's, and the Portuguese coast (Fig. 1).
91 France and Spain are considered to be tectonically stable on Holocene timescales (Boillot et al.,
92 1979; Morzadec-Kerfourn et al., 1995; Chaumillon et al., 2010; Delgado et al., 2012), although
93 some activity has been reported in various sites of France (Klingebliel and Gayet, 1995; Gandouin
94 et al., 2007) and northwestern Spain (Alonso Millán and Pagés Valcarlos, 2010). The Portuguese
95 coast is known for neotectonic activity (de Groot and Granja, 1998; Terrinha, 1998; Dias, 2001)
96 that has manifested as well-documented historical seismicity (Chester, 2001; Baptista et al., 2003;
97 Besana-Ostman et al., 2012).

98 The climate of the ACE, following the Köppen climate classification, varies from temperate
99 oceanic in France and northern Spain, temperate Mediterranean (with warm summers) in northwest
100 Spain and the northern half of Portugal, and warm Mediterranean (with hot summers) in the
101 southern half of Portugal. In northern France, mean annual temperature is ~10.6 °C and mean
102 annual precipitation ranges from 711 to 1085 mm (Caen and Brest stations; Muhr, 2016). In middle
103 to southern France, mean annual temperature ranges from 11.9 °C to 12.4 °C, and mean annual

104 precipitation ranges from 789 to 905 mm (Nantes and Bordeaux stations; Muhr, 2016). In northern
105 Spain, mean annual temperature ranges from 12.7 °C to 14.1 °C and mean annual precipitation
106 ranges from 971 to 1581 mm (San Sebastian, Oviedo, and A Coruña stations; Muhr, 2016). In
107 northwestern Spain and Portugal, mean annual temperature ranges from 13.4 °C to 14.8 °C and
108 mean annual precipitation ranges from 1142 to 1952 mm (Vigo and Porto stations; Muhr, 2016).
109 In mid-southern Portugal, mean annual temperature is ~17.1 °C and mean annual precipitation
110 ranges from 522 to 679 mm (Lisbon and Faro stations; Muhr, 2016).

111 Great diurnal tidal range, from mean high water springs (MHWS) to mean low water springs
112 (MLWS), along the ACE, varies from macrotidal in France (up to 11.40 m during spring tides) to
113 mesotidal regimes in northern Spain and Portugal (between 3.92 m during spring tides and 1.90 m
114 during neap tides). Tidal levels for our study sites were obtained from the nearest tide gauge from
115 each location (tide levels extracted from SHOM (2016) for France, Puertos del Estado (2013) for
116 Spain, and Admiralty Tide Tables (2015) for Portugal).

117 **3. Material and methods**

118 ***3.1 Relative sea level (RSL) reconstruction***

119 A sea-level index point estimates the position of RSL at a single point in space and time (Shennan
120 and Horton, 2002). Where a suite of sea-level index points exists for a locality or region, they
121 describe changes in RSL through time and can be used to estimate rates of change (Engelhart et
122 al., 2011). A sea-level index point is a datum that contains information about the geographical
123 position, elevation, indicative meaning, and age of a sample. The methodology that is employed

124 to produce valid sea-level index points is described in ‘The Manual of Sea-level Research’
125 (Shennan et al., 2015) and many other publications (e.g., Shennan, 1986; van de Plassche, 1986;
126 Engelhart and Horton, 2012).

127 *3.1.1 Vertical position of RSL*

128 To produce a sea-level index point, the indicative meaning of a dated sample must be estimated
129 (Shennan and Horton, 2002). The indicative meaning of a sample describes the relationship of the
130 environment in which it accumulated relative to a contemporaneous reference tide level (van de
131 Plassche, 1986). The indicative meaning varies according to the type of sea-level indicator and it
132 is commonly expressed in terms of an indicative range (IR) and a reference water level (RWL)
133 (Horton et al., 2000). The former is a vertical range within which the coastal sample may occur
134 and the latter a water level to which the sample is related, for example, mean higher high water
135 (MHHW), mean tide level (MTL), etc. (Shennan et al., 2015). To allow for sea-level trends to be
136 inferred from multiple types of sea-level indicators and for comparisons to be made between
137 different areas, each sample is related to its own reference tide level (Shennan, 1986).

138 Indicative meanings for the ACE database (Table 1) were estimated using published and
139 unpublished data relating the distribution of modern salt-marsh, estuarine and lagoonal samples to
140 elevation with respect to the tidal frame (Cearreta, 1998; Fatela et al., 2009; Stéphan et al., 2015a;
141 Camacho et al., 2017). Within a salt marsh, it is usually possible to observe a clear vertical division
142 of plants into high marsh and low marsh zones, which reflects the preferences and tolerances of
143 halophytic species to the frequency and duration of tidal inundation (Kemp et al., 2010). The high
144 to middle marsh environments in France and Spain are generally covered by *Halimione*

145 *portulacoides*, *Juncus maritimus*, *Scirpus maritimus*, and *Elymus pycnanthus* vegetation; the low
146 marsh is represented by *Spartina maritima*, *Salicornia ramosissima*, and *Puccinellia maritima*
147 halophytic vegetation (Benito and Onaindia, 1991; Stéphan et al., 2015a). In southern Portugal,
148 the high marsh is dominated by *Sarcocornia perennis* spp. *Alpine* and *Suaeda vera*, and the middle
149 marsh by *H. portulacoides* and *Spartina densiflora*. The low marsh is dominated by *S. perennis*
150 spp. *perennis* and *S. maritima*, as well as taxa found in the middle marsh (Camacho et al., 2017).

151 Similarly, studies of salt-marsh microfossils, such as foraminifera, diatom, pollen and ostracods,
152 have shown that assemblages have characteristic preferences for particular elevations in the
153 intertidal zone (Schneider et al. 2010; Horton et al., 2006; Kemp et al., 2009). Similar to Engelhart
154 and Horton (2012), we inferred that samples identified to be from salt-marsh origin formed
155 between highest astronomical tide (HAT) and MTL. If preserved plant macrofossils (e.g., reed
156 fragments) or microfossils (e.g., foraminifera) suggested a high marsh environment, an IR of HAT
157 to mean high water (MHW) was assigned to the sample. For low marsh environments, the IR
158 applied was MHW to MTL. Pollen assemblages were used to identify an undifferentiated salt-
159 marsh environment when halophilous taxa were found in organic sediment.

160 Some index points from Portugal were derived from lagoonal/shallow marine samples that were
161 classified as either open or semi-enclosed environments based on the presence of certain articulate
162 bivalve, ostracoda, and foraminifera taxa. We applied the same indicative meanings suggested by
163 Vacchi et al. (2016) for these lagoonal samples of MTL to -2 m (open) and MTL to -1 m (enclosed),
164 except for samples that contained the articulated bivalves *Cerastoderma glaucum* and *Loripes*
165 *lacteus*. According to Teixeira et al. (2005) these species are infra-littoral taxa and can live > 2 m
166 below MTL in the Algarve region, so they were considered as marine limiting dates. Finally, we

167 adopted a broad indicative meaning for those samples with a mixture of marine and brackish water
168 indicators that we classified as an undifferentiated intertidal environment, between HAT and mean
169 low water (MLW).

170 Where biostratigraphic data indicated formation and deposition in a freshwater or marine
171 environment, the sample was classified as a limiting date. Reconstructed RSL must fall below
172 freshwater limiting dates and above marine limiting dates. Although limiting dates cannot
173 constrain the precise position of past sea level, they are extremely important in understanding and
174 interpreting sea-level changes, as well as constraining GIA models (e.g., Shennan and Horton,
175 2002; Engelhart and Horton, 2012).

176 Freshwater limiting dates form at an elevation above the tidal influence, commonly above HAT;
177 however, these depositional environments may possibly be linked to rising groundwater, and
178 therefore we used a RWL of above MTL (Jelgersma, 1961; Shennan et al., 2000; Engelhart and
179 Horton, 2012). Freshwater limiting dates from the ACE were derived from organic sediment
180 samples with freshwater indicators (e.g., Gabet, 1973; Tastet et al., 2000) or fluvial sediments
181 where marine indicators were absent (e.g., García-Artola et al., submitted).

182 Marine limiting dates form below MTL. The majority of marine limiting dates from the ACE were
183 retrieved from estuarine muddy or sandy environments with a very low organic matter content
184 (i.e., tidal flat). Previous regional RSL reconstructions (i.e., Leorri et al., 2012a; Stéphan and
185 Goslin, 2014) had interpreted tidal flat sediments as index points, but we plotted them as marine
186 limiting dates because it is often difficult to determine the lower limit of these environments.
187 Where possible, we used dates from marine shells recovered in living position (e.g., Teixeira et

188 al., 2005). We eliminated those samples recovered from depositional environments highly prone
189 to remobilization (e.g., channel bottom sediments).

190 The mean estimate of RSL for each index point was calculated as:

$$191 \text{RSL}_i = E_i - \text{RWL}_i \quad [1]$$

192 where E_i and RWL_i are the elevation and reference water level of sample i , expressed relative to
193 the same tidal datum (e.g., MTL). For a modern (surface) sample, the terms E_i and RWL_i are equal,
194 thus RSL will be zero. All index points in the database are expressed in relation to this value,
195 where negative values indicate RSL below present.

196 Elevation within the ACE was commonly established by referring the samples to an orthometric
197 datum by means of a total station or a GPS. Sometimes this information was not available, and we
198 estimated the elevation based on the local vegetation referenced to mean sea level (MSL),
199 measured at the nearest tide gauge.

200 *3.1.2 Sources of uncertainty for the vertical position of RSL*

201 The uncertainty for the vertical position of RSL takes into account many sources of uncertainty
202 and can be quantified following Shennan and Horton (2002). Apart from the uncertainty associated
203 with the indicative meaning (i.e., the IR), there are a series of additional uncertainties related to
204 the determination of the depth of a sample in the core and the elevation of the core. To determine
205 the uncertainty associated with the sample depth, we have taken into account the sample thickness
206 (measured or estimated), the sampling uncertainty, the compaction associated with the sampling
207 method, and the angle of the borehole that decreases with depth. To determine the uncertainty

208 associated with calculating the elevation of a sample, we considered the tidal range and water
209 depth for samples obtained offshore, the uncertainty of the total station, GPS or Real Time
210 Kinematic (RTK), and the benchmark for high-precision surveying. When these uncertainties were
211 not specified in the original publications, we used the recommended values by Hijma et al. (2015)
212 shown in Table 2. We assigned an uncertainty of half the tidal range for samples where the
213 orthometric elevation was reported but the methodology was unknown (e.g., Frouin et al., 2009;
214 Gandouin et al., 2009). For elevations estimated from the local vegetation, we adopted an
215 uncertainty of half the vertical distribution of the depositional environment (e.g., undifferentiated
216 salt marsh). We did not apply any corrections for tidal range variation in the past.

217 An additional form of uncertainty for the vertical position of RSL is post-depositional lowering
218 due to compaction of underlying sediment. This unidirectional process causes the underestimation
219 of the RSL position. In order to qualitatively evaluate the possible influence of compaction, we
220 have divided the sea-level index points into basal and intercalated (Horton and Shennan, 2009),
221 but we have not quantified the uncertainty associated with compaction. Basal samples are derived
222 from sediments lying directly above an incompressible substrate, while the intercalated samples
223 are susceptible to compaction because they are located between non-basal clastic sediments
224 (Jelgersma, 1961). In addition, we have only considered freshwater limiting dates coming from
225 basal sediments to avoid high-limiting constraints affected by compaction plotting below sea-level
226 index points.

227 *3.1.3 Age and uncertainty of RSL*

228 All sea-level index points and limiting dates were radiocarbon dated (Accelerator Mass
229 Spectrometry, AMS or radiometric) and expressed as calibrated years before present (BP,
230 measured with respect to 1950 CE). All dates obtained prior to the mid-1980s were corrected for
231 isotopic fractionation following Stuiver et al. (2017). When $\delta^{13}\text{C}$ values were not reported, we
232 assigned standard values (-27‰ for terrestrial and 0‰ for marine samples). To account for the
233 possibility of multiple sources of carbon supply in bulk sediment samples (e.g., freshwater, salt-
234 marsh, or tidal flat bulk organic/minerogenic sediment), we added an additional uncertainty of \pm
235 100 years (Hu, 2010).

236 We calibrated all index points and limiting dates using CALIB 7.1 (Stuiver et al., 2017) with a 2σ
237 confidence interval. Terrestrial samples (e.g., wood fragment, freshwater and salt-marsh peat)
238 were calibrated using the IntCal13 calibration curve (Reimer et al., 2013). Marine samples (e.g.,
239 bivalve shells and calcareous foraminifera) were calibrated using the Marine 13 calibration curve
240 (Reimer et al., 2013). For samples dated using *Hydrobia* shells, we applied the mixed Marine and
241 Northern Hemisphere Atmosphere curve (Reimer et al., 2013) for calibration following Billeaud
242 (2007). For marine samples, we used the following average (spatial and temporal) local marine
243 reservoir corrections (ΔR): -7 ± 50 years (Tisnérat-Laborde et al., 2010) for the French Atlantic
244 coast (regions #1, #3, #6, and #7); -105 ± 21 years (Monge Soares et al., 2016) for the Cantabrian
245 Sea (region #8); -192 ± 24 years (Monge Soares and Dias, 2007) for the northern Galician coast
246 (region #10); 95 ± 15 years (Monge Soares and Dias, 2006) for the central Portuguese coast (region
247 #12); and 69 ± 17 years (Martins and Monge Soares, 2013) for the southwest Portuguese coast
248 (region #13). We do not show local marine reservoir corrections from coastal regions that were
249 dated using only terrestrial materials.

250 3.1.4 Example of a sea-level index point from northern Spain

251 A sea-level index point (SLIP) was recovered from the Anbeko salt marsh located in the lower-
252 middle Urdaibai estuary (northern Spain) (Fig. 2), which has subsequently been reclaimed for
253 cattle grazing (García-Artola et al., submitted). We extracted a 4.80 m sediment core using a rotary
254 drill. We measured the surface elevation of the core using a GPS-RTK (± 0.02 m leveling
255 uncertainty), which was tied into a benchmark (± 0.10 m estimated benchmark uncertainty) to
256 which the tidal datum is referenced. The core surface elevation was 1.81 ± 0.12 m NMMA (or
257 MSL in Alicante, Spanish orthometric datum defined in the Mediterranean coast) or 1.50 ± 0.12
258 m MSL at the nearest Bilbao tide gauge (located on the Atlantic coast and consequently used in
259 this study). The stratigraphy showed a sandy sediment at the base dominated by estuarine
260 calcareous foraminifera species that evolved into a silty sediment with an exclusively agglutinated
261 foraminiferal assemblage at the top.

262 A small halophytic plant remain was selected at a depth of 2.72 m (-1.22 m MSL) for AMS dating.
263 The AMS dated plant remain (Beta-463064) yielded a calibrated age of 4421 to 4248 cal BP, which
264 represents the horizontal 2σ range of the SLIP.

265 The foraminiferal assemblage at this depth was dominated by the agglutinated species *Entzia*
266 *macrescens* (90%), *Trochammina inflata* (6%), and *Arenoparrella mexicana* (4%) that are typical
267 of a high marsh environment. The RWL of the sample was calculated as the midpoint between
268 HAT and MHW, and the IR uncertainty as half the elevation difference between HAT and MHW.
269 The elevation of HAT and MHW is 2.39 m MSL and 1.36 m MSL, respectively, at the nearest tide
270 gauge (Bilbao). Therefore, the sample's RWL is 1.87 m MSL and the IR is 1.03 m, with an

271 associated IR uncertainty of ± 0.52 m. We calculated the total uncertainty for this sample from the
272 following uncertainty terms: sample thickness uncertainty of ± 0.01 m; non-vertical drilling
273 uncertainty of ± 0.01 m; core shortening uncertainty of ± 0.15 m; and a standard sampling
274 uncertainty of ± 0.01 m.

275 The calculation of RSL and its uncertainty for this index point was:

$$276 \text{ RSL} = -1.22 \text{ m}_{\text{elevation}} - 1.87 \text{ m}_{\text{RWL}} = -3.09 \text{ m}$$

$$277 \text{ RSL uncertainty} = \pm [(0.52 \text{ m})^2_{\text{IR}} + (0.12 \text{ m})^2_{\text{elevation}} + (0.01 \text{ m})^2_{\text{sample thickness}} + (0.01 \text{ m})^2_{\text{angle borehole}} \\ 278 + (0.15 \text{ m})^2_{\text{coring method}} + (0.01 \text{ m})^2_{\text{sampling}}]^{1/2} = 0.55 \text{ m}$$

279 ***3.2 Statistical Analysis***

280 We fit the RSL index points with a spatio-temporal empirical hierarchical model (Ashe et al., in
281 rev.; Cressie and Wikle, 2011; Kopp et al., 2016). As a hierarchical model, it separately
282 distinguishes between variability at the process level in the underlying spatio-temporal RSL field
283 and noise introduced at the data level, through geochronological uncertainty, vertical measurement
284 uncertainty, and the IR. Prior expectations about scales of variability are described by
285 hyperparameters, which in an empirical model are optimized to maximize the likelihood of the
286 model given the observations.

287 The process level decomposes the spatio-temporal field of RSL change, $f(\mathbf{x},t)$, into four
288 components, representing (1) a slowly changing signal common to the region of study, $g(t)$, (2) a
289 long-wavelength regional signal, $r(\mathbf{x},t)$, (3) a short-wavelength regional signal, $s(\mathbf{x},t)$, and (4) high-
290 frequency, localized variability, represented as white noise, $w(\mathbf{x},t)$:

291
$$f(\mathbf{x}, t) = g(t) + r(\mathbf{x}, t) + s(\mathbf{x}, t) + w(\mathbf{x}, t) \quad [2]$$

292 The data level represents each individual RSL estimate y_i and age observation \hat{t}_i as a noisy
293 corruption of true RSL and true age, $f(\mathbf{x}, t_i)$ and t_i :

294
$$y_i = f(\mathbf{x}_i, t_i) + \varepsilon_i \quad [3]$$

295
$$\hat{t}_i = t_i + \delta_i \quad [4]$$

296 Geochronological uncertainties are approximated using the Noisy-Input Gaussian Process
297 approximation (McHutchon and Rasmussen, 2011).

298 Each of the terms on the right-hand side of equation [2] is characterized by a mean-zero Gaussian-
299 process prior with Matérn covariance (once differentiable for temporal covariances [Matérn-3/2]
300 and not differentiable for spatial covariances [Matérn-1/2]) (Rasmussen and Williams, 2006). The
301 optimized hyperparameters are shown in Table 3. Standard deviations for the vertical and temporal
302 uncertainty terms in equations [3] and [4] are defined in the database. The optimized
303 hyperparameters indicate that the more local terms ($s(\mathbf{x}, t)$ and $w(\mathbf{x}, t)$) contribute minimally to the
304 overall signal (Table 3); almost all deviations from the common signal and the longer-wavelength
305 regional signal can be explained by individual sample uncertainty.

306 **4. Holocene relative sea-level records of the Atlantic Coast of Europe**

307 ***4.1 French Flanders and Picardy coastal plain (region #1)***

308 The RSL history consists of 16 index points from organic sediment from former salt-marsh
309 environments, eight marine limiting dates, and eight freshwater limiting dates (Fig. 3). In the early

310 Holocene, between ~ 10.4 ka and ~ 9.3 ka, freshwater limiting dates constrain RSL to below -21.1
311 ± 3.3 m. The oldest index point places RSL at -17.7 ± 3.8 m at ~ 8.6 ka. Then, RSL rose to $-11.8 \pm$
312 3.8 m at ~ 7.5 ka at a rate of 5.7 ± 1.2 mm yr⁻¹. There is an absence of index points between ~ 7.5
313 and ~ 5.7 ka, but a freshwater limiting date constrains RSL to below -3.1 ± 4.2 m at ~ 7.1 ka.
314 Younger index points show a RSL rise from -3.3 ± 3.8 m at ~ 5.7 ka to -1.8 ± 3.3 m at ~ 2 ka at a
315 rate of 1.2 ± 0.5 mm yr⁻¹. Two marine limiting dates indicate RSL was above 0.1 ± 2.7 m between
316 ~ 1.5 and ~ 1.2 ka.

317 ***4.2 Seine estuary and Coast of Calvados (region #2)***

318 The RSL record contains 20 index points from salt-marsh organic sediment and one freshwater
319 limiting date (Fig. 3). A freshwater limiting date constrains RSL to below -22.3 ± 3.4 m at ~ 9.5
320 ka. The oldest index point places RSL at -20.2 ± 3.9 m at ~ 8.9 ka. A basal index point suggests
321 RSL was at -10.8 ± 3.9 m at ~ 8.2 ka, and then it rose to -7.2 ± 3.9 m at ~ 6.9 ka at 4.3 ± 1.0 mm yr⁻¹
322 and to -6.5 ± 3.9 m at ~ 6.2 ka at a rate of 2.3 ± 0.8 mm yr⁻¹. Intercalated index points show RSL
323 remained relatively stable during the late Holocene, reaching -0.2 ± 3.6 m at ~ 4.4 ka, although
324 four index points suggest RSL was $\sim -2.0 \pm 1.8$ m between ~ 2.6 and ~ 2.2 ka.

325 ***4.3 Normano-breton Gulf and North Brittany (region #3)***

326 The RSL record is based on 24 salt marsh-based index points, three marine limiting dates, and four
327 freshwater limiting dates (Fig. 3). The oldest freshwater limiting date indicates RSL was below -
328 9.1 ± 5.4 m at ~ 8.1 ka. Mainly basal index points show RSL rose from -8.7 ± 5.9 m at ~ 7.5 ka to -
329 5.7 ± 5.9 m at ~ 6.9 ka at a rate of 3.4 ± 1.1 mm yr⁻¹, and to -2.9 ± 5.9 m at ~ 5 ka at a rate of $1.5 \pm$

330 0.5 mm yr⁻¹. During the late Holocene, data are scarce, and a single index point places RSL at 0.0
331 ± 5.9 m at ~3 ka. Finally, a marine limiting date indicates RSL was above -1.9 ± 5.7 m at ~1 ka.

332 ***4.4 West Brittany (region #4)***

333 The West Brittany RSL record is composed of 28 index points from salt-marsh organic sediment
334 and seven freshwater limiting dates (Fig. 3). The oldest basal index point locates RSL at -7.5 ± 0.8
335 m at ~6.9 ka. A series of basal and intercalated index points show RSL rose relatively steadily to
336 -0.4 ± 0.8 m at ~0.5 ka at a rate of 1.0 ± 0.2 mm yr⁻¹.

337 ***4.5 South Brittany (region #5)***

338 The RSL record from South Brittany contains 14 index points from salt-marsh organic sediment,
339 four marine limiting dates and three freshwater limiting dates (Fig. 3). A marine limiting date
340 suggests RSL was above -8.6 ± 0.2 m at ~7.9 ka. The oldest basal index point places RSL at -6.7
341 ± 2.8 m at ~7.5 ka. RSL rose from -5.2 ± 2.8 m at ~6.5 ka to -2.8 ± 3.0 m at ~5.2 ka at a rate of
342 1.0 ± 0.5 mm yr⁻¹. A freshwater limiting date constrains RSL to below -0.5 ± 2.1 m at ~4.3 ka.
343 During the late Holocene, RSL remained relatively stable at -1.2 ± 1.4 m to -1.3 ± 3.0 m between
344 ~3.9 and ~1.2 ka.

345 ***4.6 Coast of Vendée (region #6)***

346 The RSL record is derived from 32 index points from undifferentiated tidal sediments and salt-
347 marsh organic sediment (Fig. 3). The oldest index point in the early Holocene places RSL at -9.2
348 ± 2.7 m at ~8.9 ka. However, the next two index points locate RSL at ~-10 m at ~8.6 ka. RSL rose

349 until ~ 7.9 ka at a rate of 6.7 ± 1.2 mm yr⁻¹, when it reached -5.5 ± 2.7 m. Then, RSL evolved from
350 -5.0 ± 2.7 m at ~ 7.1 ka to the modern position at ~ 5.1 ka at a rate of 1.1 ± 0.4 mm yr⁻¹. Even
351 though the general trend of the late Holocene RSL record shows an average position close to
352 modern, there are 3 index points at ~ 4.9 ka, ~ 4.7 ka, and ~ 3.7 ka that suggest RSL was between –
353 2.1 ± 2.7 and -2.8 ± 3.2 m.

354 ***4.7 Coast of Charentes (region #7)***

355 The RSL record is made of 11 index points, six marine limiting dates, and two freshwater limiting
356 dates (Fig. 3). The oldest freshwater limiting date constrains RSL to below -13.1 ± 2.6 m at ~ 9 ka.
357 Two marine limiting dates place RSL above -11.1 ± 2.6 m at ~ 8.5 ka and above -9.5 ± 2.6 m at
358 ~ 8.1 ka. The oldest index point indicates RSL was at -5.2 ± 2.9 m at ~ 7.3 ka. RSL rose to $-3.5 \pm$
359 2.9 m at ~ 7.1 ka. Then, RSL evolved from -3.0 ± 2.9 m at ~ 6.5 ka to -1.5 ± 2.6 m at ~ 4.7 ka at a
360 rate of 0.7 ± 0.5 mm yr⁻¹. The late Holocene is only constrained by three index points that place
361 RSL at $\sim -1.0 \pm 2.5$ m at ~ 2.9 ka and at 0.5 ± 2.8 m at ~ 0.6 ka.

362 ***4.8 Basque Country (region #8)***

363 The Basque Country RSL record consists of 12 index points from salt-marsh organic sediments,
364 47 marine limiting dates, and three freshwater limiting dates (Fig. 4). Even though marine limiting
365 dates from shells recovered from the eastern Cantabrian coast have previously shown signs of
366 reworking because of the high-energy coastal activity (Alonso and Pagés, 2000; Cearreta and
367 Murray, 2000), we used them here to constrain RSL because they are currently the only available
368 material prior to ~ 5 ka. The RSL record from the early and mid-Holocene is derived from

369 freshwater and marine limiting dates. Three freshwater limiting dates constrain RSL to below ~
370 25 m at ~9.8 ka. A series of marine limiting dates show RSL rose from above -21.6 m at ~9.4 ka
371 to above -8.5 m at ~8 ka. Marine limiting dates indicate RSL evolved from above -5.9 m at ~7.5
372 ka to above -4.2 m at ~6.7 ka. There is a lack of data between ~6.7 and ~5.8 ka. Two marine
373 limiting dates indicate RSL was above ~-5.8 m between ~5.7 and ~5.3 ka. The oldest index point
374 places RSL at -3.3 ± 0.5 m at ~4.9 ka. RSL continued to rise at a rate of 0.4 ± 0.3 mm yr⁻¹ during
375 the late Holocene until ~1.6 ka, when it reached -2.1 ± 0.5 m.

376 ***4.9 Asturias (region #9)***

377 The RSL record includes six index points from organic sediments of salt-marsh origin and three
378 marine limiting dates (Fig. 4). The oldest marine limiting date indicates RSL was above -10.1 m
379 at ~8.2 ka. The oldest index point shows RSL was located at 7.1 ± 2.3 m at ~7.5 ka. Five younger
380 index points indicate RSL rose from -5.5 ± 2.3 m at ~6.1 ka to -1.4 ± 2.3 m at ~1.2 ka at a rate of
381 0.6 ± 0.3 mm yr⁻¹.

382 ***4.10 Galicia (region #10)***

383 The RSL record for Galicia is composed of five index points from salt-marsh organic sediment,
384 eight marine limiting dates, and one freshwater limiting date (Fig. 4). Two marine limiting dates
385 constrain RSL to above -38.2 m at ~10.9 ka and -36.2 m at ~10.6 ka. An early Holocene basal
386 index point suggests RSL was at -21.7 ± 2.3 m at ~9.6 ka. RSL rose from -9.5 ± 2.1 m at ~8.4 ka
387 to -4.1 ± 2.1 m at ~7 ka at a rate of 4.7 ± 0.8 mm yr⁻¹. During the late Holocene, one freshwater
388 and three marine limiting dates constrain RSL to below -0.7 ± 1.8 m at ~5 ka and to above $-3.2 \pm$

389 1.8 m at ~4.4 ka and -1.0 m at ~3.1 ka. Younger index points show RSL rose from -1.8 ± 2.1 m
390 at ~2 ka to -0.2 ± 2.1 m at ~0.9 ka at a rate of 0.6 ± 0.7 mm yr⁻¹.

391 ***4.11 Southern Galicia and north of Portugal (region #11)***

392 The RSL record contains eight index points from salt-marsh and lagoonal organic sediments, four
393 marine limiting dates, and four freshwater limiting dates (Fig. 4). The early and mid-Holocene
394 record is constrained only by marine and freshwater limiting dates. Marine limiting dates suggest
395 RSL was above -22.7 ± 1.3 m at ~10.4 ka, -20.6 ± 1.3 m at ~10 ka, -6.7 ± 0.4 m at ~7.6 ka and -
396 5.4 ± 0.4 m at ~6.5 ka. Freshwater limiting dates suggest RSL was below -13.9 ± 1.3 m at ~10.8
397 ka, -4.2 ± 0.1 m at ~7.8 ka, -1.0 ± 1.4 m at ~6.7 ka and -1.2 ± 0.1 m at ~6 ka. The late Holocene
398 RSL record derived from intercalated index points demonstrates RSL remained close to present,
399 from -1.6 ± 1.1 m at ~2.4 ka to -0.2 ± 0.6 m at ~0.4 ka.

400 ***4.12 Lisbon and Tagus Valley (region #12)***

401 The RSL history is constrained by 17 index points from salt-marsh and lagoonal organic sediments,
402 and four marine limiting dates (Fig. 4). The oldest basal index point indicates RSL was located at
403 -36.7 ± 1.2 m at ~11.5 ka. RSL then rose to -2.4 ± 1.7 m at ~7.5 ka at a rate of 8.1 ± 0.7 mm yr⁻¹
404 and to -1.6 ± 1.2 m at ~6.9 ka at a rate of 3.4 ± 1.0 mm yr⁻¹. A younger basal index point places
405 RSL at -0.9 ± 1.2 m at ~6.3 ka. There is little information of the late Holocene RSL evolution. A
406 basal and a younger intercalated index point indicate RSL rose from -1.6 ± 1.6 m at ~4.1 ka to -
407 1.5 ± 1.5 m at ~1.5 ka at a rate of 0.0 ± 0.5 mm yr⁻¹.

408 **4.13 Algarve (region #13)**

409 The Algarve RSL record is derived from 21 index points from lagoonal muds and sands, four
410 marine limiting dates, and two freshwater limiting dates (Fig. 4). The oldest index point constrains
411 RSL to -10.7 ± 1.7 m at ~ 8.5 ka. RSL rose to -3.6 ± 1.7 m at ~ 7.2 ka at a rate of 5.3 ± 0.6 mm yr⁻¹.
412 ¹. Later, a series of index points indicate RSL rose from -2.5 ± 0.5 m at ~ 6.4 ka to 0.4 ± 0.9 m at
413 ~ 1 ka at a rate of 0.5 ± 0.2 mm yr⁻¹.

414 **5. Discussion**

415 **5.1 RSL reconstructions from the Atlantic coast of Europe**

416 The Holocene RSL database for the ACE is made up of 214 index points and 126 limiting dates
417 extracted from estuaries, coastal lagoons and salt marshes (Fig. 1). Most RSL reconstructions are
418 derived from intercalated index points from salt-marsh and occasionally lagoonal sediments
419 (regions #10-13) that extend back to ~ 11.5 ka. There are only 40 basal index points that are mainly
420 distributed between ~ 7 and ~ 5 ka. The general lack of basal data from the early Holocene has also
421 been noticed in other RSL databases such as the Mediterranean (Vacchi et al., 2016). Data are
422 limited during the early Holocene because of restricted peat formation and preservation during
423 periods of rapid RSL rise, as well as the difficulty in retrieving these coastal sediments, which
424 occur mainly offshore (Brooks and Edwards, 2006; Törnqvist and Hijma, 2012). When the rate of
425 the marine transgression slowed down (~ 7 ka), the modern coastline and estuaries formed
426 (Teixeira et al., 2005; Vis et al., 2008; Stéphan and Goslin, 2014), with basal peats occupying the
427 base of the coastal sequences. Subsequently the estuaries of the ACE infilled with tidal flat and

428 salt-marsh sediments deposited mainly during the mid- and late Holocene (Boski et al., 2002; Vis
429 and Kasse, 2009; Chaumillon et al., 2010; Fenies et al., 2010; Menier et al., 2010). This
430 stabilization of RSL in the mid to late Holocene is reflected by the formation of coastal barriers,
431 due to sediment transport along the coastline, and development of lagoons in low-lying coastal
432 areas of Portugal (Dias et al., 2000; Cearreta et al., 2003; Freitas et al., 2003; Naughton et al.,
433 2007) and France (Lespez et al., 2010; Stéphan and Laforge, 2013; Stéphan et al., 2015a, 2015b).

434 Subdivision of index points within the ACE into basal and intercalated categories provides an
435 initial assessment of the influence of compaction (e.g., Törnqvist et al., 2008; Horton and Shennan,
436 2009). However, there is no difference in the elevation between basal and intercalated index points
437 in regions #2, 3 and 4, which have data covering the same time period (Fig. 3). These results
438 contradict conclusions made from coastal organic sediments of eastern and southwestern England
439 (Edwards, 2006; Horton and Shennan, 2009), and the Gulf coast of United States (Törnqvist et al.,
440 2008), which show long-term compaction rates between ~ 0.4 and 5 mm yr^{-1} . Furthermore, Horton
441 et al. (2013) and Khan et al. (2017) assessed the influence of compaction in organic sediments
442 from temperate salt marshes and tropical mangroves in terms of their stratigraphic position and
443 showed $\sim 0.3 \text{ m}$ compaction per meter of overburden. RSL reconstructions from intercalated
444 samples in regions #2 and 3 from the ACE exhibit up to 8 and 9 m overburden, respectively, but
445 do not seem to have suffered significant consolidation. Compaction parameters such as pore space,
446 de-watering, structural collapse or biological decay of vegetal remains, and biogeochemical
447 alteration of organic matter (van Asselen et al., 2009; Brain et al., 2017) are controlled both directly
448 and indirectly by organic matter content (Plater et al., 2015). The coastal sediments of the ACE
449 are more minerogenic compared to the UK and especially North America (Cearreta et al., 2013;

450 García-Artola et al., 2016). Natural and regenerated salt-marsh sediments from the ACE contain
451 low organic matter content (<10%), which decreases with depth due to rapid degradation at the
452 surface (Cearreta et al., 2002, 2013; Santín et al., 2009; Fernández et al., 2010), compared to the
453 organic-rich salt marshes of the US Atlantic coast (e.g., >40% organic matter in New England;
454 Carey et al., 2017).

455 *5.2 Rate of RSL rise during the Holocene from the Atlantic coast of Europe*

456 The database from the ACE documents a continuous rise in RSL from -36.7 ± 1.2 m at ~ 11.5 ka
457 until present (region #12; Fig. 4). The height of RSL did not exceed the current position at any
458 time during the Holocene, although Moura et al. (2007) suggested a RSL highstand occurred
459 during the mid-Holocene in southern Portugal. We analyzed the temporal variability of RSL rise
460 for each site calculating the average rate in time intervals of 1-ka (Table 4 and Fig. 5) using the
461 spatio-temporal empirical hierarchical model (Kopp et al., 2016). Rates of Holocene RSL rise were
462 faster in the early Holocene (10 to 7 ka) with rates between 6.3 ± 0.8 mm yr⁻¹ and 6.8 ± 0.5 mm
463 yr⁻¹, and a notable decrease in rates at 7 ka. This inflection in the rate of RSL rise was also observed
464 by Vis et al. (2008), Leorri et al. (2012a,b), Stéphan and Goslin (2014), and Costas et al. (2016).
465 The rate of RSL rise further decreased from the mid to late Holocene; from 7 to 4 ka RSL rise
466 ranged from 1.8 ± 0.5 mm yr⁻¹ to 0.5 ± 0.4 mm yr⁻¹ compared to 0.9 ± 0.4 mm yr⁻¹ to 0.1 ± 0.5 mm
467 yr⁻¹ between 4 ka and present. The rate of RSL rise decreased throughout the Holocene because of
468 a reduction in meltwater input and diminishing contribution of GIA (Engelhart and Horton, 2012).
469 The decrease in rates of RSL rise after ~ 7 ka coincides with the disappearance of the far-field
470 Laurentide Ice Sheet (Carlson et al., 2008; Lambeck et al., 2014; Ullman et al., 2016), and the

471 deglaciation peak of West Greenland (Sinclair et al., 2016). However, there is no consensus on the
472 termination of Holocene global meltwater input, which has been associated with melting from the
473 Antarctic Ice Sheet after ~7 ka (Nakada and Lambeck, 1988; Ivins and James, 2005; Bentley et
474 al., 2014). This varies between 6 ka (Milne et al., 2005) and 4 ka (Peltier, 2004), or a much later
475 melting up to 2 ka (Nakada and Lambeck, 1988; Fleming et al., 1998; Whitehouse et al., 2012;
476 Lambeck et al., 2014), and 1 ka (Ivins et al., 2013; Bradley et al., 2016).

477 *5.3 Spatial variability in RSL and comparison with Glacial Isostatic model predictions*

478 The spatial variability of RSL along the ACE seems to be driven by the deglaciation of the British-
479 Irish and Fennoscandian Ice sheets (Carlson and Clark, 2012; Cuzzone et al., 2016). The ACE
480 database seems to reflect the migration of the European peripheral forebulge from the northeast to
481 the northwest during the Holocene (Fig. 5). From 8 to 4 ka, RSL rise rates decrease towards the
482 southwest from a maximum of 2.5 ± 0.5 mm yr⁻¹ (region #1) to a minimum of 1.5 ± 0.4 mm yr⁻¹
483 (regions #8-12) (Table 4). After 4 ka, the rate of RSL rise decreases from the northwest (0.9 ± 0.4
484 mm yr⁻¹: region #4) to a minimum of 0.1 ± 0.5 mm yr⁻¹ (region #12). These results confirm previous
485 conclusions showing highest RSL rates associated with the peak forebulge collapse occurring in
486 distal locations, up to hundreds of kilometers away from the former ice margins (Engelhart and
487 Horton, 2012; Engelhart et al., 2015). Data from regions #12 and 13 do not follow the general
488 north-south trend and present higher rates to the south in region #13 (Fig. 5). Previous regional
489 studies in Algarve/Gulf of Cadiz area have also suggested anomalously high rates of Holocene
490 RSL rise (Dabrio et al., 2000; Delgado et al., 2012). Consequently, RSL records from the southern

491 region of Portugal could be influenced by the previously mentioned late Quaternary tectonic
492 activity as suggested by Leorri et al. (2012a,b).

493 GIA model predictions have been compared to RSL reconstructions from the ACE (Leorri et al.,
494 2012a,b; Goslin et al., 2015; Costas et al., 2016). Similar to Bradley et al. (2011), the predictions
495 of the GIA model used here (Bradley et al., 2016 with the rheological parameters from Leorri et
496 al., 2012) compare favorably at most regions during the Holocene. However, misfits are observed
497 before ~7 ka in regions #6, 10, 12, and 13; the RSL reconstruction is up to ~10 m below GIA
498 model predictions at ~9 ka in region #6 (Fig. 3). Furthermore, region #8 also shows late Holocene
499 RSL reconstructions ~2.5 m below the GIA model predictions (Fig. 4). However, many salt
500 marshes from the Basque Country studied in this database have suffered land drainage related to
501 reclamation for agricultural purposes (e.g., Pascual et al., 2000), which would have contaminated
502 the RSL reconstructions in this area (Shennan and Horton, 2002).

503 Other possible causes of discrepancies between the RSL records and GIA model predictions have
504 been extensively discussed in previous studies (Leorri et al., 2012a,b; Goslin et al., 2015). These
505 differences could be caused by changes in paleo-tidal ranges at regional (continental shelf) and
506 local (bay, estuary) scales (region #4), tectonic activity (region #13), and large morphological
507 coastal changes (region #7). Otherwise, uncertainties in GIA models employed have been pointed
508 out, such as the choice of parameters for the Earth model used (especially the lithosphere thickness
509 and mantle viscosity structure) and the deglaciation history of the Fennoscandian ice sheet (Goslin
510 et al., 2015).

511 **6. Conclusions**

512 This work represents the first standardized Holocene RSL database from the ACE that synthesizes
513 the existing results from northern France to southern Portugal. The database is based upon 214
514 index points and 126 limiting dates that extend back to ~11.5 ka. The ACE represents an
515 intermediate-field location with a continuous Holocene RSL rise history controlled by isostatic
516 and eustatic factors. We observed the highest rates of RSL change in the early Holocene (10 to 7
517 ka) with a maximum in middle Portugal ($6.8 \pm 0.5 \text{ mm yr}^{-1}$) and a minimum in southwestern France
518 ($6.3 \pm 0.8 \text{ mm yr}^{-1}$). Reduction of meltwater input explains the slowdown in the rates after 7 ka,
519 up to $0.1 \pm 0.5 \text{ mm yr}^{-1}$ in middle Portugal during the late Holocene. The spatial variability of the
520 ACE database reflects the deglaciation of the British-Irish and Fennoscandian Ice Sheets and the
521 migration of the peripheral forebulge from a northeast position before ~4 ka to a northwest location
522 in the late Holocene.

523 **Acknowledgments**

524 AGA received a postdoctoral grant from the Basque Government (POS-2014-1-51). AC and AGA
525 were supported by Antropicosta (MINECO, CGL2013-41083-P), Harea-Coastal Geology
526 Research Group (EJ/GV, IT976-16) and Quaternary Unit for Research and Education (UPV/EHU,
527 UFI11/09) grants. REK was supported in part by NSF grants OCE-1458904 and OCE-1702587.
528 BPH was supported by the National Research Foundation Singapore and the Singapore Ministry
529 of Education under the Research Centres of Excellence initiative. We are grateful to Professor
530 Glenn A. Milne for providing GIA predictions and helpful comments on the manuscript. We also
531 thank Ángela Alonso and José Luis Pagés, former professors at the Universidade de A Coruña, for
532 providing their data from Asturias and Galicia and assisting us in the reinterpretation of their

533 previous results to follow the standards of the database. This paper is a contribution to INQUA
534 Project 1601P, IGCP Projects 588 and 639, PALSEA, Earth Observatory of Singapore (#) and
535 Geo-Q Zentroa Research Unit (paper #48 of the Joaquín Gómez de Llarena Laboratory).

536 **Appendix. Supplementary data**

537 Supplementary data related to this article can be found at

538 **References**

539 Admiralty Tide Tables, 2015. Europe (excluding United Kingdom and Ireland), Mediterranean
540 Sea and Atlantic Ocean. United Kingdom Hydrographic Office, volume 2, Taunton.

541 Alonso, A., Pagés, J.L., 2000. El registro sedimentario del final del Cuaternario en el litoral
542 noroeste de la Península Ibérica. Márgenes cantábrico y atlántico. Revista de la Sociedad
543 Geológica de España 13, 17-29.

544 Alonso Millán, A., Pagés Valcarlos, J.L., 2010. Evolución del nivel del mar durante el Holoceno
545 en el noroeste de la Península Ibérica. Revista de la Sociedad Geológica de España 23, 157-167.

546 Ashe, E.L., Cahill, N., Hay, C.C., Khan, N.S., Kemp, A.C., Engelhart, S.E., Horton, B.P., Parnell,
547 A.C., Kopp, R.E., in rev. Statistical modeling of rates and trends in sea level. Quaternary Science
548 Reviews.

549 Bao, R., Freitas, M.d.C., Andrade, C., 1999. Separating eustatic from local environmental effects:
550 a late-Holocene record of coastal change in Albufeira Lagoon, Portugal. The Holocene 9, 341-352.

551 Baptista, M.A., Miranda, J.M., Chierici, F., Zitellini, N., 2003. New study of the 1755 earthquake
552 source based on multi-channel seismic survey data and tsunami modeling *Natural Hazards and*
553 *Earth System Sciences* 3, 333-340.

554 Benito, I., Onaindia, M., 1991. Estudio de la distribución de las plantas halófilas y su relación con
555 los factores ambientales en la marisma de Mundaka-Urdaibai. Implicaciones en la gestión del
556 medio natural. *Cuadernos de Sección (Ciencias Naturales) de Eusko Ikaskuntza* 8, 1-116.

557 Bentley, M.J., Ó Cofaigh, C., Anderson, J.B., Conway, H., Davies, B., Graham, A.G.C.,
558 Hillenbrand, C.-D., Hodgson, D.A., Jamieson, S.S.R., Larter, R.D., Mackintosh, A., Smith, J.A.,
559 Verleyen, E., Ackert, R.P., Bart, P.J., Berg, S., Brunstein, D., Canals, M., Colhoun, E.A., Crosta,
560 X., Dickens, W.A., Domack, E., Dowdeswell, J.A., Dunbar, R., Ehrmann, W., Evans, J., Favier,
561 V., Fink, D., Fogwill, C.J., Glasser, N.F., Gohl, K., Golledge, N.R., Goodwin, I., Gore, D.B.,
562 Greenwood, S.L., Hall, B.L., Hall, K., Hedding, D.W., Hein, A.S., Hocking, E.P., Jakobsson, M.,
563 Johnson, J.S., Jomelli, V., Jones, R.S., Klages, J.P., Kristoffersen, Y., Kuhn, G., Leventer, A.,
564 Licht, K., Lilly, K., Lindow, J., Livingstone, S.J., Massé, G., McGlone, M.S., McKay, R.M.,
565 Melles, M., Miura, H., Mulvaney, R., Nel, W., Nitsche, F.O., O'Brien, P.E., Post, A.L., Roberts,
566 S.J., Saunders, K.M., Selkirk, P.M., Simms, A.R., Spiegel, C., Stollendorf, T.D., Sugden, D.E., van
567 der Putten, N., van Ommen, T., Verfaillie, D., Vyverman, W., Wagner, B., White, D.A., Witus,
568 A.E., Zwartz, D., 2014. A community-based geological reconstruction of Antarctic Ice Sheet
569 deglaciation since the Last Glacial Maximum. *Quaternary Science Reviews* 100, 1-9.

570 Besana-Ostman, G.M., Vilanova, S.P., Nemser, E.S., Falcao-Flor, A., Heleno, S., Ferreira, H.,
571 Fonseca, J.D., 2012. Large Holocene Earthquakes in the Lower Tagus Valley Fault Zone, Central
572 Portugal. *Seismological Research Letters* 83, 67-76.

573 Billeaud, I., 2007. Dynamique de construction d'un prisme sédimentaire littoral en régime
574 mégatidal (la Baie du Mont-Saint-Michel). Thèse de Doctorat, Université de Caen Basse
575 Normandie, Caen, p. 239.

576 Boillot, G., Dupeuble, P.A., Malod, J., 1979. Subduction and tectonics on the continental margin
577 off northern Spain. *Marine Geology* 32, 53-70.

578 Boski, T., Moura, D., Veiga-Pires, C., Camacho, S., Duarte, D., Scott, D.B., Fernandes, S.G., 2002.
579 Postglacial sea-level rise and sedimentary response in the Guadiana Estuary, Portugal/Spain
580 border. *Sedimentary Geology* 150, 103-122.

581 Bradley, S.L., Milne, G.A., Horton, B.P., Zong, Y., 2016. Modelling sea level data from China
582 and Malay-Thailand to estimate Holocene ice-volume equivalent sea level change. *Quaternary*
583 *Science Reviews* 137, 54-68.

584 Bradley, S.L., Milne, G.A., Shennan, I., Edwards, R., 2011. An improved Glacial Isostatic
585 Adjustment model for the British Isles. *Journal of Quaternary Science* 26, 541-552.

586 Brain, M.J., Kemp, A.C., Hawkes, A.D., Engelhart, S.E., Vane, C.H., Cahill, N., Hill, T.D.,
587 Donnelly, J.P., Horton, B.P., 2017. Exploring mechanisms of compaction in salt-marsh sediments
588 using Common Era relative sea-level reconstructions. *Quaternary Science Reviews* 167, 96-111.

589 Brooks, A., Edwards, R., 2006. The Development of a Sea-Level Database for Ireland. Irish
590 Journal of Earth Sciences 24, 13-27.

591 Camacho, S., Boski, T., Moura, D., Scott, D., Connor, S., Pereira, L., 2017. Paleoenvironmental
592 evolution of the Guadiana Estuary, Portugal, during the Holocene: A modern foraminifera analog
593 approach. *The Holocene* 27, 197-235.

594 Carey, J.C., Moran, S.B., Kelly, R.P., Kolker, A.S., Fulweiler, R.W., 2017. The Declining Role of
595 Organic Matter in New England Salt Marshes. *Estuaries and Coasts* 40, 626-639.

596 Carlson, A.E., Clark, P.U., 2012. Ice Sheet Sources of Sea Level Rise and Freshwater Discharge
597 during the Last Deglaciation. *Reviews of Geophysics* 50, RG4007.

598 Carlson, A.E., LeGrande, A.N., Oppo, D.W., Came, R.E., Schmidt, G.A., Anslow, F.S., Licciardi,
599 J.M., Obbink, E.A., 2008. Rapid early Holocene deglaciation of the Laurentide ice sheet. *Nature*
600 *Geoscience* 1, 620.

601 Cearreta, A., 1998. Holocene sea-level change in the Bilbao estuary (north Spain): foraminiferal
602 evidence. *Micropaleontology* 44, 265-276.

603 Cearreta, A., Cachão, M., Cabral, M.C., Bao, R., Maria de Jesus, R., 2003. Lateglacial and
604 Holocene environmental changes in Portuguese coastal lagoons 2: microfossil multiproxy
605 reconstruction of the Santo André coastal area. *The Holocene* 13, 447-458.

606 Cearreta, A., García-Artola, A., Leorri, E., Irabien, M.J., Masque, P., 2013. Recent environmental
607 evolution of regenerated salt marshes in the southern Bay of Biscay: Anthropogenic evidences in
608 their sedimentary record. *Journal of Marine Systems* 109, S203-S212.

609 Cearreta, A., Irabien, M.J., Ulibarri, I., Yusta, I., Croudace, I.W., Cundy, A.B., 2002. Recent Salt
610 Marsh Development and Natural Regeneration of Reclaimed Areas in the Plentzia Estuary, N.
611 Spain. *Estuarine, Coastal and Shelf Science* 54, 863-886.

612 Cearreta, A., Murray, J.W., 2000. AMS 14C dating of Holocene estuarine deposits: consequences
613 of high energy and reworked foraminifera. *The Holocene* 10, 155-159.

614 Chaumillon, E., Tessier, B., Reynaud, J.Y., 2010. Stratigraphic records and variability of incised
615 valleys and estuaries along French coasts. *Bulletin de la Societè Geologique de France* 181, 75-
616 85.

617 Chen, X., Zhang, X., Church, J.A., Watson, C.S., King, M.A., Monselesan, D., Legresy, B., Harig,
618 C., 2017. The increasing rate of global mean sea-level rise during 1993-2014. *Nature Climate*
619 *Change* 7, 492-495.

620 Chester, D.K., 2001. The 1755 Lisbon earthquake. *Progress in Physical Geography* 25, 363-383.

621 Church, J.A., Clark, P.U., Cazenave, A., Gregory, J.M., Jevrejeva, S., Levermann, A., Merrifield,
622 M.A., Milne, G.A., Nerem, R.S., Nunn, P.D., Payne, A.J., Pfeffer, W.T., Stammer, D.,
623 Unnikrishnan, A.S., 2013. Sea-Level Rise by 2100. *Science* 342, 1445-1445.

624 Clark, C.D., Hughes, A.L.C., Greenwood, S.L., Jordan, C., Sejrup, H.P., 2012. Pattern and timing
625 of retreat of the last British-Irish Ice Sheet. *Quaternary Science Reviews* 44, 112-146.

626 Clavé, B., Massé, L., Carbonel, P., Tastet, J.-P., 2001. Holocene coastal changes and infilling of
627 the La Perroche marsh (French Atlantic coast). *Oceanologica Acta* 24 377-389.

628 Costas, S., Ferreira, Ó., Plomaritis, T.A., Leorri, E., 2016. Coastal barrier stratigraphy for
629 Holocene high-resolution sea-level reconstruction. *Scientific Reports* 6, 38726.

630 Cressie, N., Wikle, C.K., 2011. *Statistics for spatio-temporal data*. John Wiley & Sons, Ltd,
631 Hoboken, NJ.

632 Cuzzone, J.K., Clark, P.U., Carlson, A.E., Ullman, D.J., Rinterknecht, V.R., Milne, G.A., Lunkka,
633 J.-P., Wohlfarth, B., Marcott, S.A., Caffee, M., 2016. Final deglaciation of the Scandinavian Ice
634 Sheet and implications for the Holocene global sea-level budget. *Earth and Planetary Science*
635 *Letters* 448, 34-41.

636 Dabrio, C.J., Zazo, C., Goy, J.L., Sierro, F.J., Borja, F., Lario, J., González, J.A., Flores, J.A.,
637 2000. Depositional history of estuarine infill during the last postglacial transgression (Gulf of
638 Cadiz, Southern Spain). *Marine Geology* 162, 381-404.

639 de Groot, T.A.M., Granja, H.M., 1998. Coastal Environments, Sea-Level and Neotectonism from
640 Cored Boreholes (Northwest Portugal): Preliminary Results. *Journal of Coastal Research* special
641 issue 26, 115-124.

642 Delgado, J., Boski, T., Nieto, J.M., Pereira, L., Moura, D., Gomes, A., Sousa, C., Garcia-Tenorio,
643 R., 2012. Sea-level rise and anthropogenic activities recorded in the late Pleistocene/Holocene
644 sedimentary infill of the Guadiana Estuary (SW Iberia). *Quaternary Science Reviews* 33, 121-141.

645 Dias, J.M.A., Boski, T., Rodrigues, A., Magalhaes, F., 2000. Coast line evolution in Portugal since
646 the Last Glacial Maximum until present - a synthesis. *Marine Geology* 170, 177-186.

647 Dias, R.P., 2001. Neotectónica da Região do Algarve. Unpublished PhD Thesis, Fac. Ciências,
648 Univ. Lisboa, Lisboa, 369.

649 Edwards, R.J., 2006. Mid- to late-Holocene relative sea-level change in southwest Britain and the
650 influence of sediment compaction. *Holocene* 16, 575-587.

651 Engelhart, S.E., Horton, B.P., 2012. Holocene sea level database for the Atlantic coast of the
652 United States. *Quaternary Science Reviews* 54, 12-25.

653 Engelhart, S.E., Peltier, W.R., Horton, B.P., 2011. Holocene relative sea-level changes and glacial
654 isostatic adjustment of the U.S. Atlantic coast. *Geology* 39, 751-754.

655 Engelhart, S.E., Vacchi, M., Horton, B.P., Nelson, A.R., Kopp, R.E., 2015. A sea-level database
656 for the Pacific coast of central North America. *Quaternary Science Reviews* 113, 78-92.

657 Fatela, F., Moreno, J., Moreno, F., Araújo, M.F., Valente, T., Antunes, C., Taborda, R., Andrade,
658 C., Drago, T., 2009. Environmental constraints of foraminiferal assemblages distribution across a
659 brackish tidal marsh (Caminha, NW Portugal). *Marine Micropaleontology* 70, 70-88.

660 Fenies, H., Lericolais, G., Posamentier, H.W., 2010. Comparison of wave-and tide-dominated
661 incised valleys: specific processes controlling systems tract architecture and reservoir geometry.
662 Bulletin de la Société Géologique de France 181, 171-181.

663 Fernández, S., Santín, C., Marquínez, J., Álvarez, M.A., 2010. Saltmarsh soil evolution after land
664 reclamation in Atlantic estuaries (Bay of Biscay, North coast of Spain). Geomorphology 114, 497-
665 507.

666 Fleming, K., Johnston, P., Zwartz, D., Yokoyama, Y., Lambeck, K., Chappell, J., 1998. Refining
667 the eustatic sea-level curve since the Last Glacial Maximum using far- and intermediate-field sites.
668 Earth and Planetary Science Letters 163, 327-342.

669 Freitas, M.d.C., Andrade, C., Rocha, F., Tassinari, C., Munhá, J.M., Cruces, A., Vidinha, J., Silva,
670 C.M.d., 2003. Lateglacial and Holocene environmental changes in Portuguese coastal lagoons 1:
671 the sedimentological and geochemical records of the Santo André coastal area. The Holocene 13,
672 433-446.

673 Frouin, M., Durand, A., Sebag, D., Huault, M.-F., Ogier, S., Verrecchia, E.P., Laignel, B., 2009.
674 Holocene evolution of a wetland in the Lower Seine Valley, Marais Vernier, France. The Holocene
675 19, 717-727.

676 Gabet, C., 1973. Le banc de tourbe sur l'estran de la baie de Perroche (Île d'Oléron). Recueil de
677 la Société d'Archéologie et d'Histoire de la Charente Maritime 25, 297-307.

678 Gandouin, E., Ponel, P., Andrieu-Ponel, V., Guiter, F., de Beaulieu, J.-L., Djamali, M., Franquet,
679 E., Van Vliet-Lanoë, B., Alvitre, M., Meurisse, M., Brocandel, M., Brulhet, J., 2009. 10,000 years

680 of vegetation history of the Aa palaeoestuary, St-Omer Basin, northern France. Review of
681 Palaeobotany and Palynology 156, 307-318.

682 Gandouin, E., Van Vliet Lanoë, B., Franquet, E., Andrieu-Ponel, V., Keen, D.H., Ponel, P. ,
683 Meurisse, M., Brulhet, J., Brocandel, M., 2007. Analyse en haute résolution de l'enregistrement
684 de la transgression holocène dans un secteur subsident du littoral français : le bassin-marais de
685 Saint-Omer (Pas-de-Calais, France). Géologie de la France 1, 11-32.

686 García-Artola, A., Cearreta, A., Horton, B.P., Monge-Ganuzas, M., Pérez-Díaz, S., Nikitina, D.,
687 submitted. Holocene evolution of the Oka estuary, Urdaibai Biosphere Reserve, northern Spain:
688 Response to sea-level variation. Palaeogeography, Palaeoclimatology, Palaeoecology.

689 García-Artola, A., Cearreta, A., Irabien, M.J., Leorri, E., Sanchez-Cabeza, J.-A., Corbett, D.R.,
690 2016. Agricultural fingerprints in salt-marsh sediments and adaptation to sea-level rise in the
691 eastern Cantabrian coast (N. Spain). Estuarine, Coastal and Shelf Science 171, 66-76.

692 García-Artola, A., Cearreta, A., Leorri, E., 2015. Relative sea-level changes in the Basque coast
693 (northern Spain, Bay of Biscay) during the Holocene and Anthropocene: The Urdaibai estuary
694 case. Quaternary International 364, 172-180.

695 Goslin, J., Van Vliet Lanoë, B., Spada, G., Bradley, S., Tarasov, L., Neill, S., Suanez, S., 2015. A
696 new Holocene relative sea-level curve for western Brittany (France): Insights on isostatic
697 dynamics along the Atlantic coasts of north-western Europe. Quaternary Science Reviews 129,
698 341-365.

699 Goslin, J., Van Vliet-Lanoë, B., Stéphan, P., Delacourt, C., Fernane, A., Gandouin, E., Hénaff, A.,
700 Penaud, A., Suanez, S., 2013. Holocene relative sea-level changes in western Brittany (France)
701 between 7600 and 4000 cal. BP: Reconstitution from basal-peat deposits. *Geomorphologie: Relief,*
702 *Processus, Environnement*, 425-444.

703 Hernández Martín, S., 2013. Evolución ambiental de los estuarios vascos (Urdaibai y Deba)
704 durante el Holoceno como consecuencia del ascenso del nivel marino. *Estudios de Cuaternario*
705 *CKQ 3*, 51-63.

706 Hijma, M.P., Engelhart, S.E., Törnqvist, T.E., Horton, B.P., Hu, P., Hill, D.F., 2015. A protocol
707 for a geological sea-level database, *Handbook of Sea-Level Research*. John Wiley & Sons, Ltd,
708 Chichester, pp. 536-553.

709 Hinkel, J., Jaeger, C., Nicholls, R.J., Lowe, J., Renn, O., Peijun, S., 2015. Sea-level rise scenarios
710 and coastal risk management. *Nature Climate Change 5*, 188-190.

711 Horton, B.P., Corbett, R., Culver, S.J., Edwards, R.J., Hillier, C., 2006. Modern saltmarsh diatom
712 distributions of the Outer Banks, North Carolina, and the development of a transfer function for
713 high resolution reconstructions of sea level. *Estuarine, Coastal and Shelf Science 69*, 381-394.

714 Horton, B.P., Edwards, R.J., Lloyd, J.M., 2000. Implications of a microfossil-based transfer
715 function in Holocene sea-level studies. *Geological Society, London, Special Publications 166*, 41-
716 54.

717 Horton, B.P., Engelhart, S.E., Hill, D.F., Kemp, A.C., Nikitina, D., Miller, K.G., Peltier, W.R.,
718 2013. Influence of tidal-range change and sediment compaction on Holocene relative sea-level
719 change in New Jersey, USA. *Journal of Quaternary Science* 28, 403-411.

720 Horton, B.P., Gibbard, P., Mine, G., Morley, R., Purintavaragul, C., Stargardt, J., 2005. Holocene
721 sea levels and palaeoenvironments, Malay-Thai Peninsula, southeast Asia. *The Holocene* 15,
722 1199-1213.

723 Horton, B.P., Shennan, I., 2009. Compaction of Holocene strata and the implications for relative
724 sea-level change on the east coast of England. *Geology* 37, 1083-1086.

725 Hu, P., 2010. Developing a quality-controlled postglacial sea-level database for coastal Louisiana
726 to assess conflicting hypotheses of Gulf Coast sea-level change. MSc thesis, Tulane University.

727 Huault, M.F., 1980. Nouvelles recherches palynologiques sur le Marais Vernier. *Bulletin de*
728 *l'Association Française pour l'Etude du Quaternaire* 17, 53-56.

729 Huault, M.F., 1985 Apports des diatomées à la reconstitution des paléoenvironnements : l'exemple
730 du Marais Vernier lors de la transgression flandrienne. *Bulletin de l'Association Française pour*
731 *l'Etude du Quaternaire* 22, 209-217.

732 Ivins, E.R., James, T.S., 2005. Antarctic glacial isostatic adjustment: a new assessment. *Antarctic*
733 *Science* 17, 541-553.

734 Ivins, E.R., James, T.S., Wahr, J., O. Schrama, E.J., Landerer, F.W., Simon, K.M., 2013. Antarctic
735 contribution to sea level rise observed by GRACE with improved GIA correction. *Journal of*
736 *Geophysical Research: Solid Earth* 118, 3126-3141.

737 Jelgersma, S., 1961. *Holocene sea level changes in the Netherlands*. Van Aelst, Maastricht.

738 Joly, C., 2004 *Histoire végétale d'une tourbière littorale : le marais des Bourbes (Olonnesur-Mer,*
739 *Vendée)*. *Annales de Paléontologie* 90, 187-207.

740 Joly, C., Visset, L., 2009. Evolution of vegetation landscapes since the Late Mesolithic on the
741 French West Atlantic coast. *Review of Palaeobotany and Palynology* 154 124-179.

742 Kemp, A.C., Horton, B.P., Corbett, D.R., Culver, S.J., Edwards, R.J., van de Plassche, O., 2009.
743 The relative utility of foraminifera and diatoms for reconstructing late Holocene sea-level change
744 in North Carolina, USA. *Quaternary Research* 71, 9-21.

745 Kemp, A.C., Vane, C.H., Horton, B.P., Culver, S.J., 2010. Stable carbon isotopes as potential sea-
746 level indicators in salt marshes, North Carolina, USA. *The Holocene* 20, 623-636.

747 Khan, N., Ashe, E., Shaw, T., Vacchi, M., Walker, J., Peltier, W.R., Kopp, R., Horton, B., 2015.
748 *Holocene Relative Sea-Level Changes from Near-, Intermediate-, and Far-Field Locations*.
749 *Current Climate Change Reports* 1, 247-262.

750 Khan, N.S., Ashe, E., Horton, B.P., Dutton, A., Kopp, R.E., Brocard, G., Engelhart, S.E., Hill,
751 D.F., Peltier, W.R., Vane, C.H., Scatena, F.N., 2017. Drivers of Holocene sea-level change in the
752 Caribbean. *Quaternary Science Reviews* 155, 13-36.

753 Klingebiel, A., Gayet, J., 1995. Fluvio-lagoonal sedimentary sequences in Leyre delta and
754 Arcachon bay, and Holocene sea level variations, along the Aquitaine coast (France). *Quaternary*
755 *International* 29, 111-117.

756 Kopp, R., Hay, C., Little, C., Mitrovica, J., 2015. Geographic Variability of Sea-Level Change.
757 *Current Climate Change Reports*, 1-13.

758 Kopp, R.E., Kemp, A.C., Bittermann, K., Horton, B.P., Donnelly, J.P., Gehrels, W.R., Hay, C.C.,
759 Mitrovica, J.X., Morrow, E.D., Rahmstorf, S., 2016. Temperature-driven global sea-level
760 variability in the Common Era. *Proceedings of the National Academy of Sciences USA* 113,
761 E1434-1441.

762 Lambeck, K., Rouby, H., Purcell, A., Sun, Y., Sambridge, M., 2014. Sea level and global ice
763 volumes from the Last Glacial Maximum to the Holocene. *Proceedings of the National Academy*
764 *of Sciences USA* 111, 15296-15303.

765 Lambeck, K., Smither, C., Johnston, P., 1998. Sea-level change, glacial rebound and mantle
766 viscosity for northern Europe. *Geophysical Journal International* 134, 102-144.

767 Leorri, E., Cearreta, A., Milne, G., 2012a. Field observations and modelling of Holocene sea-level
768 changes in the southern Bay of Biscay: implication for understanding current rates of relative sea-
769 level change and vertical land motion along the Atlantic coast of SW Europe. *Quaternary Science*
770 *Reviews* 42, 59-73.

771 Leorri, E., Fatela, F., Drago, T., Bradley, S.L., Moreno, J., Cearreta, A., 2012b. Lateglacial and
772 Holocene coastal evolution in the Minho estuary (N Portugal): Implications for understanding sea-
773 level changes in Atlantic Iberia. *The Holocene* 23, 353-363.

774 Lespez, L., Clet-Pellerin, M., Davidson, R., Hermier, G., Carpentier, V., Cador, J.-M., 2010.
775 Middle to Late Holocene landscape changes and geoarchaeological implications in the marshes of
776 the Dives estuary (NW France). *Quaternary International* 216, 23-40.

777 Love, R., Milne, G.A., Tarasov, L., Engelhart, S.E., Hijma, M.P., Latychev, K., Horton, B.P.,
778 Tornqvist, T.E., 2016. The contribution of glacial isostatic adjustment to projections of sea-level
779 change along the Atlantic and Gulf coasts of North America. *Earths Future* 4, 440-464.

780 Martins, J.M.M., Monge Soares, A.M., 2013. Marine Radiocarbon Reservoir Effect in Southern
781 Atlantic Iberian Coast. *Radiocarbon* 55, 1123-1134.

782 McHutchon, A., Rasmussen, C.E., 2011. Gaussian Process Training with Input Noise. *Advances*
783 *in Neural Information Processing Systems* 24, 1341–1349.

784 Mengel, M., Levermann, A., Frieler, K., Robinson, A., Marzeion, B., Winkelmann, R., 2016.
785 Future sea level rise constrained by observations and long-term commitment. *Proceedings of the*
786 *National Academy of Sciences USA* 113, 2597-2602.

787 Menier, D., Tessier, B., Proust, J.-N., Baltzer, A., Sorrel, P., Traini, C., 2010. The Holocene
788 transgression as recorded by incised-valley infilling in a rocky coast context with low sediment
789 supply (southern Brittany, western France). *Bulletin de la Societe Geologique de France* 181, 115-
790 128.

791 Milne, G.A., Gehrels, W.R., Hughes, C.W., Tamisiea, M.E., 2009. Identifying the causes of sea-
792 level change. *Nature Geoscience* 2, 471-478.

793 Milne, G.A., Long, A.J., Bassett, S.E., 2005. Modelling Holocene relative sea-level observations
794 from the Caribbean and South America. *Quaternary Science Reviews* 24, 1183-1202.

795 Milne, G.A., Peros, M., 2013. Data–model comparison of Holocene sea-level change in the
796 circum-Caribbean region. *Global and Planetary Change* 107, 119-131.

797 Mitrovica, J.X., Milne, G.A., 2002. On the origin of late Holocene sea-level highstands within
798 equatorial ocean basins. *Quaternary Science Reviews* 21, 2179-2190.

799 Monge Soares, A.M., Dias, J.M.A., 2006. Coastal Upwelling and Radiocarbon—Evidence for
800 Temporal Fluctuations in Ocean Reservoir Effect off Portugal During the Holocene. *Radiocarbon*
801 48, 45-60.

802 Monge Soares, A.M., Dias, J.M.A., 2007. Reservoir Effect of Coastal Waters Off Western and
803 Northwestern Galicia. *Radiocarbon* 49, 925-936.

804 Monge Soares, A.M., Gutiérrez-Zugasti, I., González-Morales, M., Matos Martins, J.M., Cuenca-
805 Solana, D., Bailey, G.N., 2016. Marine Radiocarbon Reservoir Effect in Late Pleistocene and Early
806 Holocene Coastal Waters off Northern Iberia. *Radiocarbon* 58, 869-883.

807 Morzadec-Kerfourn, M.-T., 1995. Coastline changes in the Armorican Massif (France) during the
808 Holocene. *Journal of Coastal Research special issue* 17, 197-203.

809 Moura, D., Veiga-Pires, C., Albardeiro, L., Boski, T., Rodrigues, A.L., Tareco, H., 2007. Holocene
810 sea level fluctuations and coastal evolution in the central Algarve (southern Portugal). *Marine*
811 *Geology* 237, 127-142.

812 Mrani-Alaoui, M., Anthony, E.J., 2011. New data and a morphodynamic perspective on mid- to
813 late-Holocene palaeoenvironmental changes in the French Flanders coastal plain, southern North
814 Sea. *The Holocene* 21, 445-453.

815 Muhr, B., 2016. Klimadiagramme. <http://www.klimadiagramme.de/> (accessed 14.10.17).

816 Nakada, M., Lambeck, K., 1988. The melting history of the late Pleistocene Antarctic ice sheet.
817 *Nature* 333, 36.

818 Naughton, F., Sánchez Goñi, M.F., Drago, T., Freitas, M.C., Oliveira, A., 2007. Holocene Changes
819 in the Douro Estuary (Northwestern Iberia). *Journal of Coastal Research* 23, 711-720.

820 Nicholls, R.J., Hanson, S.E., Lowe, J.A., Warrick, R.A., Lu, X., Long, A.J., 2014. Sea-level
821 scenarios for evaluating coastal impacts. *Wiley Interdisciplinary Reviews: Climate Change* 5, 129-
822 150.

823 Pascual, A., Weber, O., Rodríguez-Lázaro, J., Jouanneau, J., 2000. Evolución sedimentaria del
824 pólder Anbeko (Reserva de Urdaibai, Golfo de Vizcaya) durante el Holoceno. *Geogaceta* 28, 113-
825 116.

826 Peltier, W.R., 1996. Global sea level rise and glacial isostatic adjustment: an analysis of data from
827 the east coast of North America. *Geophysical Research Letters* 23, 717-720.

828 Peltier, W.R., 2004. Global glacial isostasy and the surface of the ice-age earth: the ice-5G (VM2)
829 model and grace. *Annual Review of Earth and Planetary Sciences* 32, 111-149.

830 Plater, A.J., Kirby, J.R., Boyle, J.F., Shaw, T., Mills, H., 2015. Loss on ignition and organic
831 content, in: Shennan, I., Long, A.J., Horton, B.P. (Eds.), *Handbook of Sea-Level Research*. John
832 Wiley & Sons, Ltd, Chichester, pp. 312-330.

833 Preuss, H., 1979. Progress in computer evaluation of sea level data within the IGCP Project no.
834 61, *Proceedings 1978 International Symposium of Coastal Evolution in the Quaternary*, pp. 104-
835 134.

836 Puertos del Estado, 2013. REDMAR: Red de Mareógrafos de Puertos del Estado. Ministerio de
837 Fomento.

838 Rasmussen, C.E., Williams, C.K.I., 2006. *Gaussian processes for machine learning*. MIT Press,
839 Cambridge, MA.

840 Reimer, P.J., Bard, E., Bayliss, A., Beck, J.W., Blackwell, P.G., Bronk Ramsey, C., Buck, C.E.,
841 Cheng, H., Edwards, R.L., Friedrich, M., Grootes, P.M., Guilderson, T.P., Haflidason, H., Hajdas,
842 I., Hatté, C., Heaton, T.J., Hoffmann, D.L., Hogg, A.G., Hughen, K.A., Kaiser, K.F., Kromer, B.,
843 Manning, S.W., Niu, M., Reimer, R.W., Richards, D.A., Scott, E.M., Southon, J.R., Staff, R.A.,
844 Turney, C.S.M., van der Plicht, J., 2013. IntCal13 and Marine13 Radiocarbon Age Calibration
845 Curves 0–50,000 Years cal BP. *Radiocarbon* 55, 1869-1887.

846 Roy, K., Peltier, W.R., 2015. Glacial isostatic adjustment, relative sea level history and mantle
847 viscosity: reconciling relative sea level model predictions for the U.S. East coast with geological
848 constraints. *Geophysical Journal International* 201, 1154-1179.

849 Santín, C., de la Rosa, J.M., Knicker, H., Otero, X.L., Álvarez, M.Á., González-Vila, F.J., 2009.
850 Effects of reclamation and regeneration processes on organic matter from estuarine soils and
851 sediments. *Organic Geochemistry* 40, 931-941.

852 Schneider, H., Höfer, D., Trog, C., Busch, S., Schneider, M., Baade, J., Daut, G., Mäusbacher, R.,
853 2010. Holocene estuary development in the Algarve Region (Southern Portugal) – A
854 reconstruction of sedimentological and ecological evolution. *Quaternary International* 221, 141-
855 158.

856 Shennan, I., 1986. Flandrian sea-level changes in the Fenland. II: Tendencies of sea-level
857 movement, altitudinal changes, and local and regional factors. *Journal of Quaternary Science* 1,
858 155-179.

859 Shennan, I., Horton, B., 2002. Holocene land-and sea-level changes in Great Britain. *Journal of*
860 *Quaternary Science* 17, 511-526.

861 Shennan, I., Lambeck, K., Horton, B., Innes, J., Lloyd, J., McArthur, J., Rutherford, M., 2000.
862 Holocene isostasy and relative sea-level changes on the east coast of England. Geological Society,
863 London, Special Publications 166, 275-298.

864 Shennan, I., Long, A.J., Horton, B.P. (Eds.), 2015. *Handbook of Sea-Level Research*. John Wiley
865 & Sons, Ltd, Chichester.

866 SHOM, 2016. Marine Altimetric References, Cotes du zéro hydrographique et niveaux
867 caractéristiques de la marée. Edition SHOM, Brest.

868 Sinclair, G., Carlson, A.E., Mix, A.C., Lecavalier, B.S., Milne, G., Mathias, A., Buizert, C.,
869 DeConto, R., 2016. Diachronous retreat of the Greenland ice sheet during the last deglaciation.
870 Quaternary Science Reviews 145, 243-258.

871 Stéphan, P., Goslin, J., 2014. Evolution du niveau marin relatif à l'Holocène le long des côtes
872 françaises de l'Atlantique et de la Manche : réactualisation des données par la méthode des "sea-
873 level index points". . Quaternaire, Association Française pour l'Etude du Quaternaire (AFEQ) 25,
874 295-312.

875 Stéphan, P., Larforge, M., 2013. Mise au point sur l'évolution géomorphologique et le devenir des
876 flèches de galets du Loc'h de Landévennec (Bretagne, France). Géomorphologie : Relief,
877 Processus, Environnement 19, 191-208.

878 Stéphan, P., Goslin, J., Paillet, Y., Manceau, R., Suanez, S., Van Vliet-Lanoë, B., Hénaff, A.,
879 Delacourt, C., 2015a. Holocene salt-marsh sedimentary infilling and relative sea-level changes in
880 West Brittany (France) using foraminifera-based transfer functions. Boreas 44, 153-177.

881 Stéphan, P., Suanez, S., Fichaut, B., 2015b. Long-, Mid- and Short-Term Evolution of Coastal
882 Gravel Spits of Brittany, France, in: Randazzo, G., Jackson, D.W.T., Cooper, J.A.G. (Eds.), Sand
883 and Gravel Spits. Springer International Publishing, Cham, pp. 275-288.

884 Stuiver, M., Reimer, P.J., Reimer, R.W., 2017. CALIB 7.1 [WWW program] at <http://calib.org/>,
885 accessed 2017-9-8.

886 Tastet, J.-P., Roussot-Larroque, J., Clavé, B., 2000. Palaeo-environmental Study Area P15: West
887 Bank of the Gironde Estuary, west coast, France, in: McInnes, R.G., Tomalin, D.J., Jakeways, J.
888 (Dir.), LIFE Environment Project: LIFE-97 ENV/UK/000510 1997-2000 Coastal change, climate
889 and instability: Final Technical Report. Isle of Wight Center for the Coastal Environment,
890 Newport, 57 p.

891 Teixeira, S.B., Gaspar, P., Rosa, M., 2005. Holocene Sea-level index points on the Quarteira Coast
892 (Algarve, Portugal), in: Freitas, M.C., Drago, T. (Eds.), Iberian Holocene paleoenvironmental
893 evolution. Proceedings Coastal Hope Conference 2005. Universidade de Lisboa, Lisboa, pp.125-
894 127.

895 Terrinha, P.A.G., 1998. Structural Geology and Tectonic Evolution of the Algarve Basin, South
896 Portugal. Unpublished PhD Thesis, Imperial College, London, 430.

897 Tisnérat-Laborde, N., Paterne, M., Métivier, B., Arnold, M., Yiou, P., Blamart, D., Raynaud, S.,
898 2010. Variability of the northeast Atlantic sea surface $\Delta^{14}\text{C}$ and marine reservoir age and the
899 North Atlantic Oscillation (NAO). *Quaternary Science Reviews* 29, 2633-2646.

900 Tooley, M.J., 1982. Sea-level changes in northern England. *Proceedings of the Geologists'*
901 *Association* 93, 43-51.

902 Tornqvist, T.E., Hijma, M.P., 2012. Links between early Holocene ice-sheet decay, sea-level rise
903 and abrupt climate change. *Nature Geoscience* 5, 601-606.

904 Törnqvist, T.E., Wallace, D.J., Storms, J.E.A., Wallinga, J., van Dam, R.L., Blaauw, M., Derksen,
905 M.S., Klerks, C.J.W., Meijneken, C., Snijders, E.M.A., 2008. Mississippi Delta subsidence
906 primarily caused by compaction of Holocene strata. *Nature Geoscience* 1, 173-176.

907 Trog, C., Hempel, R., Frenzel, P., Mausbacher, R., 2015. Holocene palaeoenvironmental changes
908 in three lagoons on the Algarve coast of Portugal. *Palaeobiodiversity and Palaeoenvironments* 95,
909 203-221.

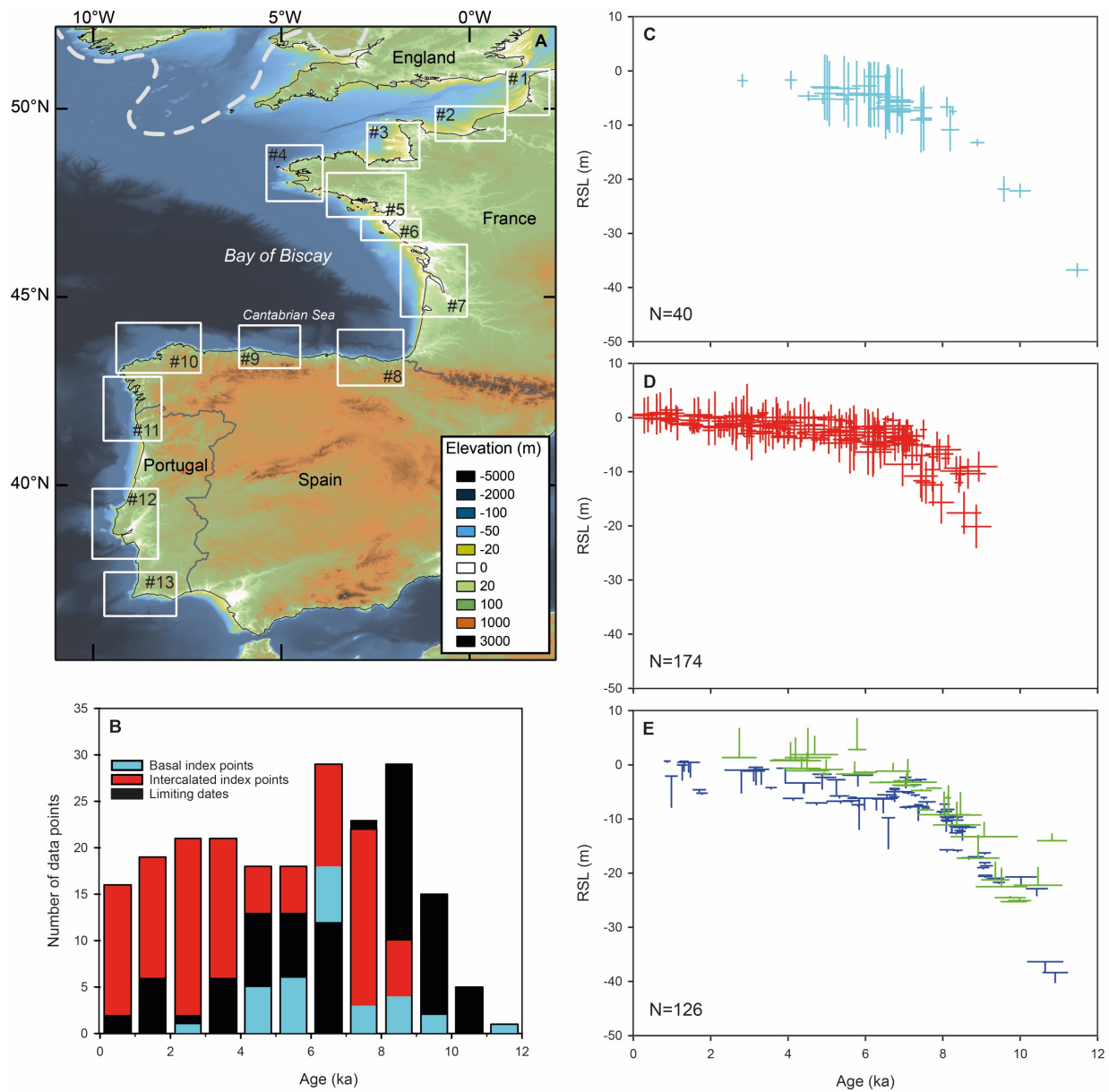
910 Trog, C., Höfer, D., Frenzel, P., Camacho, S., Schneider, H., Mäusbacher, R., 2013. A multi-proxy
911 reconstruction and comparison of Holocene palaeoenvironmental changes in the Alvor and
912 Alcantarilha estuaries (southern Portugal). *Revue de Micropaléontologie* 56, 131-158.

913 Ullman, D.J., Carlson, A.E., Hostetler, S.W., Clark, P.U., Cuzzone, J., Milne, G.A., Winsor, K.,
914 Caffee, M., 2016. Final Laurentide ice-sheet deglaciation and Holocene climate-sea level change.
915 *Quaternary Science Reviews* 152, 49-59.

916 Vacchi, M., Marriner, N., Morhange, C., Spada, G., Fontana, A., Rovere, A., 2016. Multiproxy
917 assessment of Holocene relative sea-level changes in the western Mediterranean: Sea-level
918 variability and improvements in the definition of the isostatic signal. *Earth-Science Reviews* 155,
919 172-197.

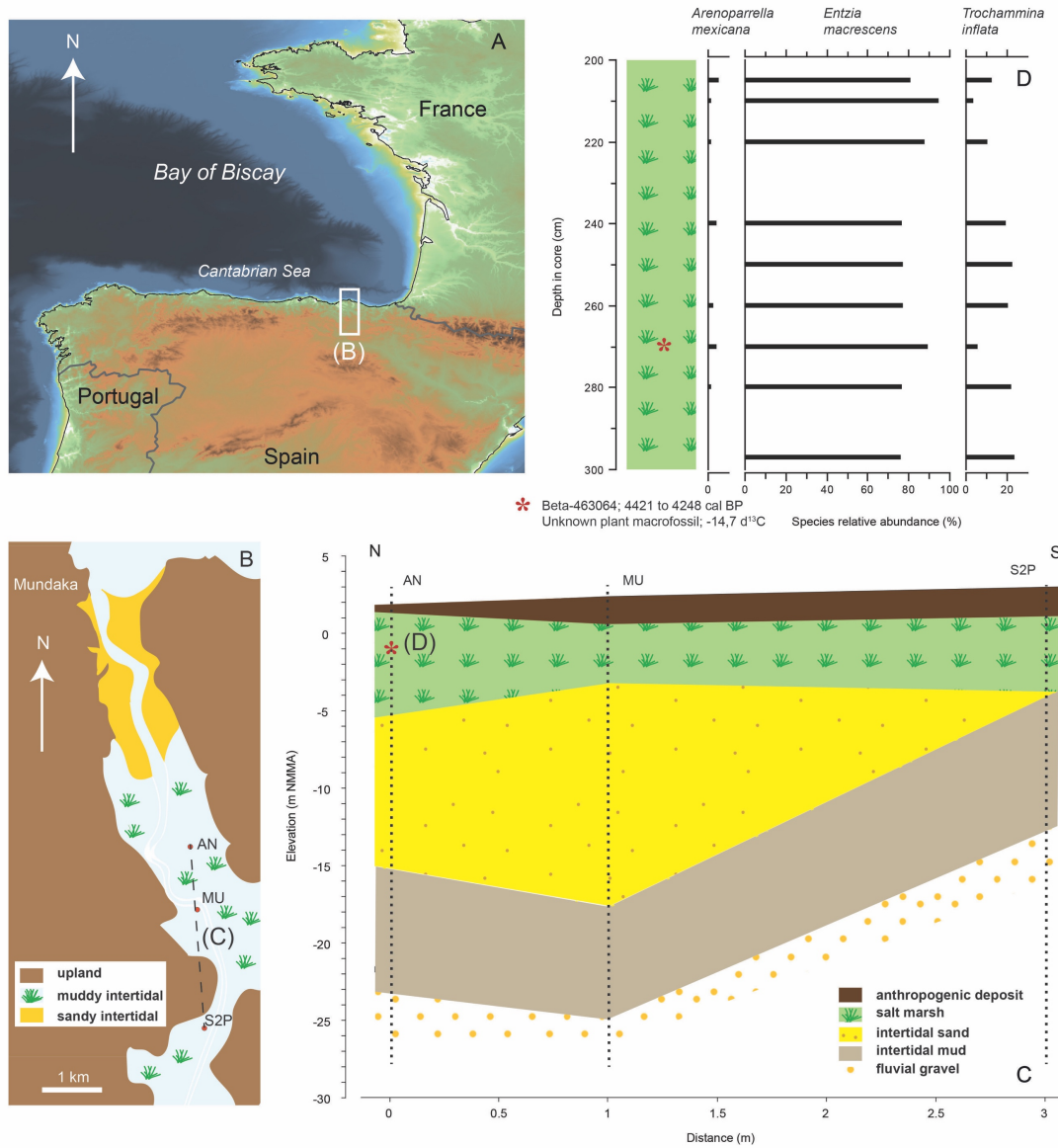
920 van Asselen, S., Stouthamer, E., van Asch, T.W.J., 2009. Effects of peat compaction on delta
921 evolution: A review on processes, responses, measuring and modeling. *Earth-Science Reviews* 92,
922 35-51.

- 923 van de Plassche, O., 1986. Sea-level Research: A Manual for the Collection and Evaluation of
924 Data. Geobooks, Norwich.
- 925 Vis, G.-J., Kasse, C., 2009. Late Quaternary valley-fill succession of the Lower Tagus Valley,
926 Portugal. *Sedimentary Geology* 221, 19-39.
- 927 Vis, G.-J., Kasse, C., Vandenberghe, J., 2008. Late Pleistocene and Holocene palaeogeography of
928 the Lower Tagus Valley (Portugal): effects of relative sea level, valley morphology and sediment
929 supply. *Quaternary Science Reviews* 27, 1682-1709.
- 930 Whitehouse, P.L., Bentley, M.J., Le Brocq, A.M., 2012. A deglacial model for Antarctica:
931 geological constraints and glaciological modelling as a basis for a new model of Antarctic glacial
932 isostatic adjustment. *Quaternary Science Reviews* 32, 1-24.



933

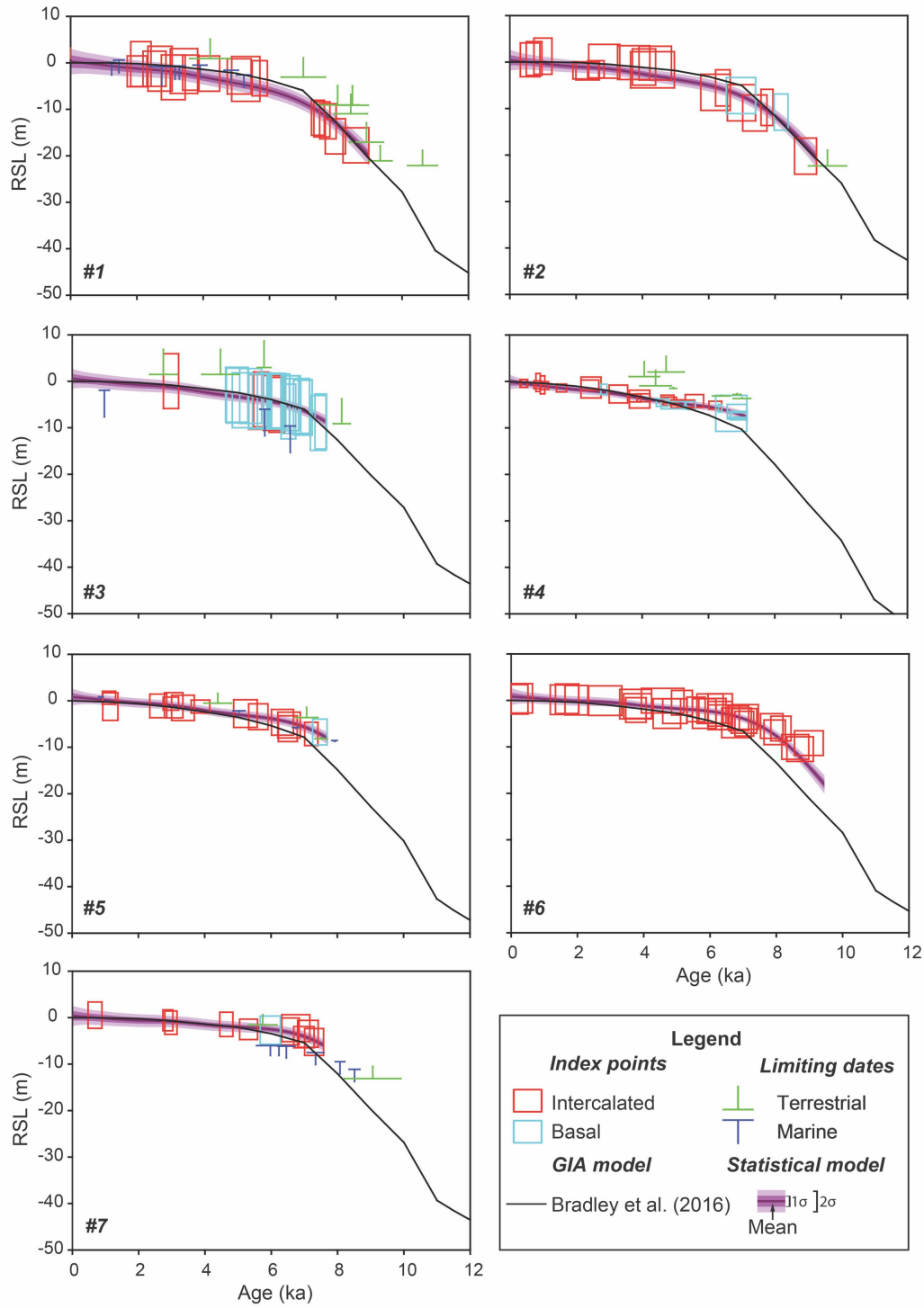
934 Fig. 1. Location map of the ACE database; dashed grey line represents the southern extent of British-Irish Ice Sheet
 935 during Last Glacial Maximum (Clark et al., 2012) (A). Number and types of data points in 1-ka time intervals (B).
 936 Temporal distribution of basal (C) and intercalated (D) index points, and limiting dates (E).



937

938 Fig. 2. Example site location in Basque Country (region #8) (A). Urdaibai estuary map with location of analyzed cores
 939 for stratigraphical purposes (B). Stratigraphic section of the middle Urdaibai estuary (C). Foraminiferal assemblage
 940 evolution throughout the 100 cm of the AN core upper section (D).

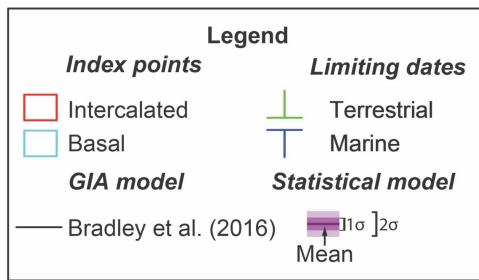
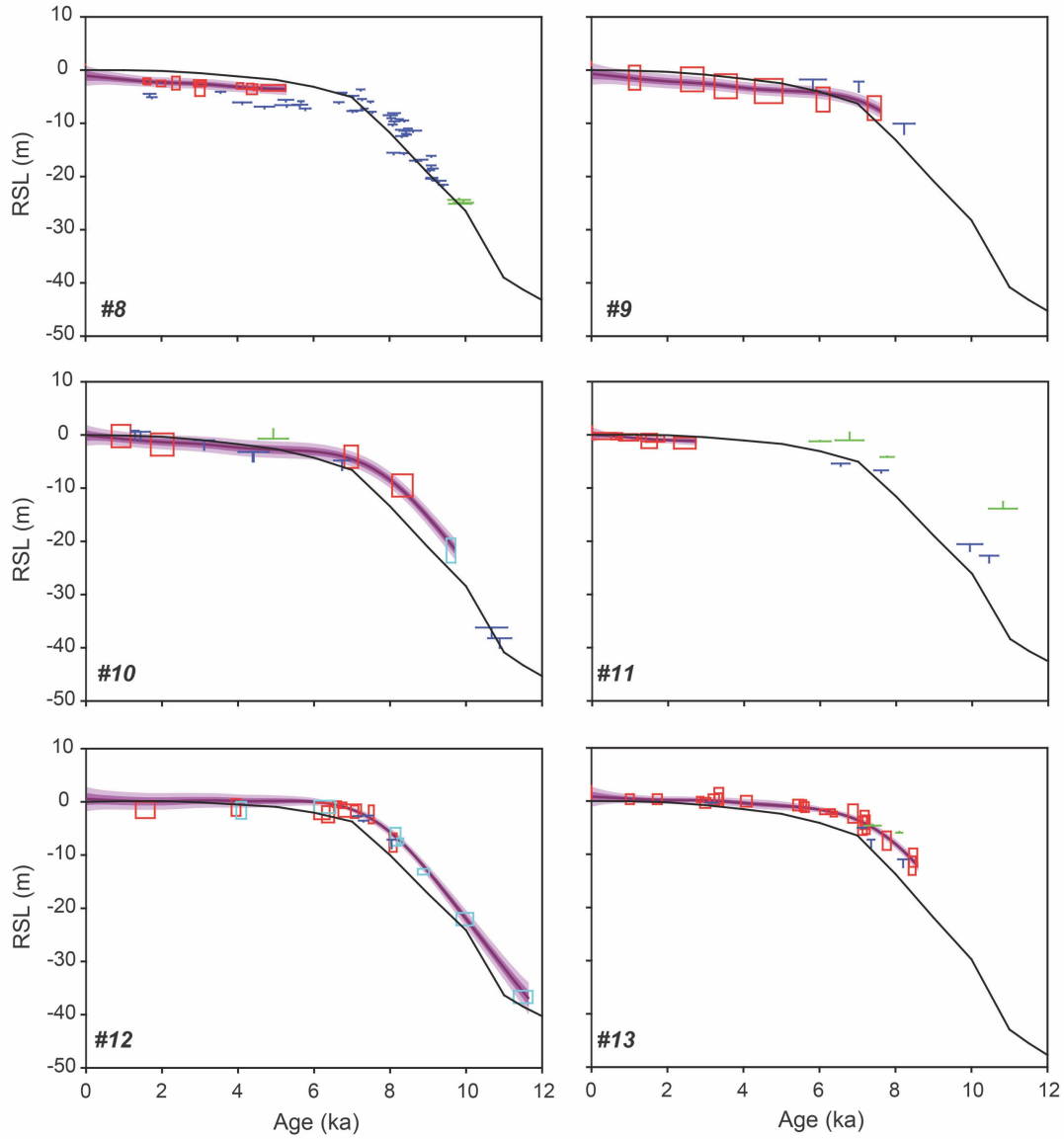
941



942

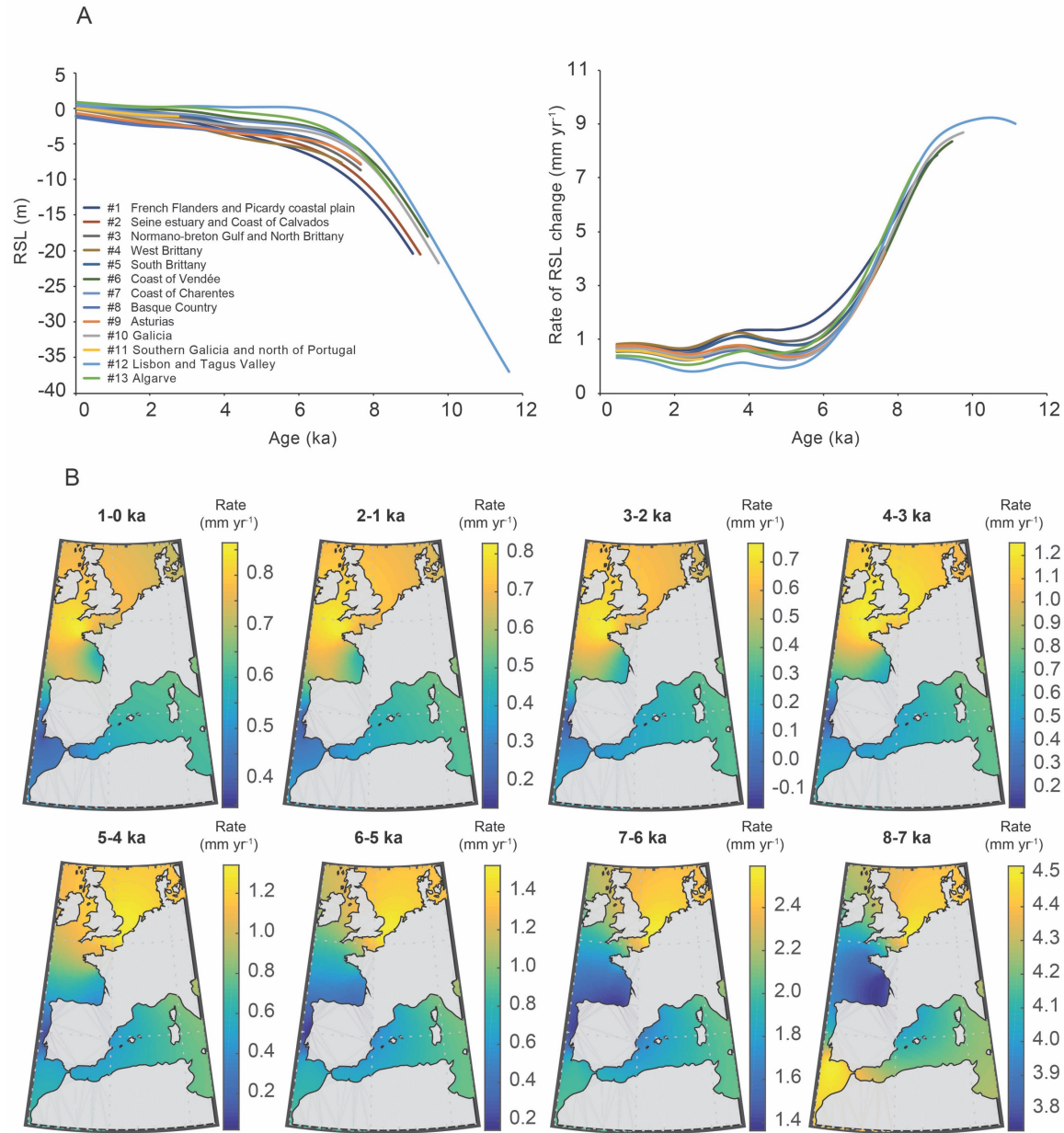
943 Fig. 3. RSL observations compared to GIA and spatio-temporal statistical model predictions for different coastal

944 regions of France.



945

946 Fig. 4. RSL observations compared to GIA and spatio-temporal statistical model predictions for different coastal
 947 regions of Spain and Portugal.



948

949 Fig. 5. Mean estimates of RSL heights and rates of change from the spatio-temporal model for each coastal region (A)

950 and rates of RSL change for the entire ACE in 1-ka time intervals (B).

951

952

953 Table 1. Definition of the indicative meanings used to develop the Atlantic coast of Europe database. HAT: highest
 954 astronomical tide. MHW: mean high water. MTL: mean tide level. MLW: mean low water.

Sample type	Evidence	Reference water level	Indicative range
Index Points			
High marsh environment	1. Foraminiferal assemblages dominated by high marsh taxa in organic and/or minerogenic sediment (e.g., Cearreta et al., 2002; Stéphan et al., 2015a; García-Artola et al., 2015). 2. Reed peat identified from plant macroremains or pollen (e.g., Goslin et al., 2013).	(HAT+MHW)/2	HAT-MHW
Low marsh environment	3. Foraminiferal assemblages dominated by low marsh taxa in a minerogenic and/or organic sediment (e.g., Tastet et al., 2000; Cearreta et al., 2002).	(MHW+MTL)/2	MHW-MTL
Undifferentiated salt-marsh environment	4. Foraminiferal assemblages dominated by high and low marsh taxa in a minerogenic and/or organic sediment or peat (e.g., Hernández Martín, 2013). 5. Pollen (with diatoms, dinoflagellates or ostracods) dominated by halophilous taxa in a minerogenic and/or organic sediment (e.g., Huault, 1980, 1985; Tastet et al., 2000; Clavé et al., 2001).	(HAT+MTL)/2	HAT-MTL
Open lagoon or shallow marine environment	6. Foraminifera, diatoms and ostracod assemblages dominated by marine and brackish littoral taxa or inner estuarine taxa (e.g., Trog et al., 2013, 2015). Articulated bivalves of intertidal taxa in life position (e.g., Teixeira et al., 2005).	-1 m	MTL to -2 m
Inner or semi-enclosed lagoon	7. Foraminifera, diatoms and ostracod assemblages dominated by brackish littoral taxa or inner estuarine taxa (e.g., Bao et al., 1999; Trog et al., 2015).	-0.5 m	MTL to -1 m
Undifferentiated intertidal environment	8. Intertidal muds with halophilous pollen species, marine shells and dinoflagellates (e.g., Joly, 2004; Joly and Visset, 2009).	(HAT+MLW)/2	HAT-MLW
Limiting Points			
Marine limiting	9. Calcareous foraminiferal assemblages and marine shells in minerogenic sediment, as well as lagoonal sediments that do not meet the requirements to be classified as index points (e.g., Cearreta, 1998; Teixeira et al., 2005; Vis et al., 2008; Mrani-Alaoui and Anthony, 2011).	MTL	Below MTL
Freshwater limiting	10. Fluvial gravels without foraminifera or marine shells (e.g., Schneider et al., 2010; García-Artola et al., submitted). 11. Pollen assemblages dominated by freshwater taxa in organic sediment (e.g., Tastet et al., 2000). 12. Freshwater shells in organic sediment (e.g., Gabet, 1973).	MTL	Above MTL

955

956 Table 2. Standardized vertical uncertainties adopted for the construction of the Atlantic coast of Europe database.

Source of error	Description
<i>Uncertainties related to the indicative meaning of a sample</i>	
Indicative range uncertainty	± indicative range/2
<i>Uncertainties related to the determination of the depth of a sample in a core</i>	
Sample thickness uncertainty*	± sample thickness/2 m
Sampling uncertainty	± 0.01 m
Core shortening/stretching uncertainty	± 0.15 m for rotary coring and vibracoring ± 0.05 m for hand coring ± 0.01 m for a Russian sampler
Non-vertical drilling uncertainty	0.02 m/m depth
<i>Uncertainties related to the determination of the elevation of a core</i>	
Offshore sample collection	
Tidal uncertainty	± tidal range/2 m
Water depth uncertainty	± 0.5 m
High-precision surveying methods	
Total station uncertainty	± 0.01 m
GPS or RTK uncertainty	± 0.1 m
Benchmark uncertainty	± 0.1 m
Unknown methods	
Tidal uncertainty	± tidal range/2 m
Estimation from vegetation zone	
Undifferentiated salt-marsh vertical distribution uncertainty	± (HAT-MTL)/2
High marsh vertical distribution uncertainty	± (HAT-MHW)/2

957 *When the sample thickness was not originally reported it was estimated from the dating method (0.1 m for AMS and

958 0.5 m for radiometric dating)

959

960

961

962

963

964

Table 3. Optimized hyperparameters

prior standard deviation of $g(t)$	78.2 m
prior timescale of $g(t)$	37.3 ka
prior standard deviation of $r(\mathbf{x},t)$	2.6 m
prior timescale of $r(\mathbf{x},t)$ and $s(\mathbf{x},t)$	6.5 ka
prior length scale of $r(\mathbf{x},t)$	13.0°
prior standard deviation of $s(\mathbf{x},t)$	0.03 m
prior length scale of $s(\mathbf{x},t)$	1.0°
prior standard deviation of $w(\mathbf{x},t)$	0.2 mm

965

966

967

968

969

970

971

972

Table 4. Rates of RSL change (± 2 standard deviations) along the ACE at 1-ka time intervals estimated by the empirical hierarchical model since 11 ka.

Site	Average rate (mm yr ⁻¹)										
	11-10 ka	10-9 ka	9-8 ka	8-7 ka	7-6 ka	6-5 ka	5-4 ka	4-3 ka	3-2 ka	2-1 ka	1-0 ka
#1 French Flanders and Picardy coastal plain	8.4 ± 2.0	8.2 ± 1.7	6.9 ± 1.4	4.5 ± 1.0	2.6 ± 0.9	1.5 ± 0.9	1.4 ± 0.8	1.2 ± 0.8	0.6 ± 0.9	0.7 ± 1.0	0.8 ± 1.7
#2 Seine estuary and Coast of Calvados	8.5 ± 2.0	8.2 ± 1.7	6.9 ± 1.3	4.3 ± 1.0	2.3 ± 0.8	1.3 ± 0.8	1.2 ± 0.7	1.1 ± 0.7	0.5 ± 0.8	0.7 ± 0.8	0.7 ± 1.6
#3 Normano-breton Gulf and North Brittany	8.6 ± 2.0	8.3 ± 1.6	6.8 ± 1.3	4.1 ± 0.9	2.0 ± 0.8	1.0 ± 0.7	1.0 ± 0.7	1.1 ± 0.7	0.5 ± 0.7	0.6 ± 0.7	0.7 ± 1.6
#4 West Brittany	8.5 ± 1.9	8.2 ± 1.6	6.7 ± 1.3	3.9 ± 1.0	1.8 ± 0.7	0.8 ± 0.6	1.0 ± 0.5	1.2 ± 0.6	0.7 ± 0.6	0.8 ± 0.6	0.8 ± 1.5
#5 South Brittany	8.7 ± 1.9	8.3 ± 1.6	6.7 ± 1.3	3.9 ± 0.9	1.8 ± 0.7	0.8 ± 0.6	0.9 ± 0.6	1.1 ± 0.6	0.5 ± 0.6	0.6 ± 0.7	0.7 ± 1.5
#6 Coast of Vendée	8.8 ± 1.9	8.4 ± 1.6	6.7 ± 1.2	3.8 ± 0.9	1.6 ± 0.7	0.6 ± 0.7	0.6 ± 0.6	0.7 ± 0.6	0.3 ± 0.6	0.4 ± 0.7	0.6 ± 1.5
#7 Coast of Charentes	8.8 ± 1.9	8.4 ± 1.6	6.8 ± 1.3	3.8 ± 0.9	1.6 ± 0.8	0.5 ± 0.8	0.5 ± 0.7	0.6 ± 0.6	0.2 ± 0.7	0.5 ± 0.8	0.6 ± 1.6
#8 Basque Country	8.8 ± 1.9	8.4 ± 1.5	6.8 ± 1.2	3.7 ± 0.9	1.4 ± 0.8	0.3 ± 0.8	0.4 ± 0.6	0.6 ± 0.5	0.3 ± 0.5	0.6 ± 0.8	0.7 ± 1.6
#9 Asturias	8.8 ± 1.8	8.4 ± 1.4	6.8 ± 1.1	3.8 ± 0.9	1.4 ± 0.8	0.4 ± 0.8	0.5 ± 0.7	0.8 ± 0.7	0.5 ± 0.7	0.7 ± 0.7	0.8 ± 1.5
#10 Galicia	8.9 ± 1.8	8.5 ± 1.4	7.0 ± 1.1	3.9 ± 0.9	1.4 ± 0.8	0.4 ± 0.8	0.4 ± 0.7	0.7 ± 0.7	0.4 ± 0.8	0.6 ± 0.7	0.7 ± 1.5
#11 Southern Galicia and north of Portugal	9.0 ± 1.8	8.6 ± 1.4	7.1 ± 1.1	4.0 ± 0.9	1.4 ± 0.8	0.3 ± 0.8	0.3 ± 0.8	0.5 ± 0.7	0.3 ± 0.7	0.5 ± 0.6	0.6 ± 1.4
#12 Lisbon and Tagus Valley	9.2 ± 1.6	8.9 ± 1.3	7.4 ± 1.0	4.2 ± 0.7	1.5 ± 0.8	0.2 ± 0.8	0.0 ± 0.7	0.1 ± 0.7	-0.2 ± 0.7	0.1 ± 0.8	0.3 ± 1.6
#13 Algarve	9.0 ± 1.7	8.8 ± 1.4	7.4 ± 1.1	4.5 ± 0.7	2.0 ± 0.7	0.7 ± 0.7	0.5 ± 0.6	0.5 ± 0.6	0.1 ± 0.6	0.3 ± 0.7	0.4 ± 1.6